Steady-State Rate-Optimal Power Adaptation in Energy Harvesting Opportunistic Cognitive Radios With Spectrum Sensing and Channel Estimation Errors

Hassan Yazdani and Azadeh Vosoughi, *Senior Member, IEEE*

***Abstract*—We consider an uplink opportunistic cognitive radio network, operating in frequency division duplexing (FDD) mode and consisting of N_{u} secondary users (SUs) and an access point (AP), that can access a spectrum band licensed to a primary user. Each SU is capable of harvesting energy, and is equipped with a finite size battery, for energy storage. The SUs operate under a time-slotted scheme, where each time slot consists of three non-overlapping phases: 1) spectrum sensing phase; 2) channel probing phase; and 3) data transmission phase. The AP feeds back its estimates of fading coefficients of SUs–AP link to SUs. To strike a balance between the energy harvesting and the energy consumption, we propose a parametrized power control strategy that allows each SU to adapt its power, according to the feedback information and its stored energy. We establish a lower bound on the achievable uplink sum-rate of SUs–AP links, in the presence of both spectrum sensing and channel estimation errors. We optimize the parameters of the proposed power control strategy, such that the derived uplink sum-rate lower bound is maximized, subject to an interference constraint. Via simulations, we corroborate our analysis and explore spectrum sensing-channel probing-data transmission trade-offs.**

***Index Terms*—Opportunistic cognitive radio, energy harvesting, imperfect spectrum sensing, channel estimation, constrained sum-rate maximization, average interference power constraint, finite-size battery, steady-state battery operation, adaptive transmission power.**

I. Introduction

A. Literature Review

THE EXPLOSIVE rise in demand for high data rate wireless applications has turned the spectrum into a scarce resource. Cognitive radio (CR) technology is a promising solution which alleviates spectrum scarcity problem by allowing an unlicensed secondary user (SU) to access licensed frequency bands in a such way that its imposed interference on primary users (PUs) is limited [1]–[3]. Therefore, CR systems can increase spectrum efficiency significantly. CR systems are mainly classified as underlay CR and opportunistic CR systems. In underlay CR systems, SUs use a licensed frequency band simultaneously with PUs, conditioned that the interference power cuased by SUs and imposed on PUs remains below a pre-determined level. In opportunistic CR systems, SUs use a licensed frequency band as long as the frequency band is not used by PUs. While opportunistic CR systems do not require coordination between PUs and SUs to acquire channel state information (CSI) corresponding to SU-PU link, they necessitate spectrum sensing to monitor and detect PUs' activities and protect PUs against harmful interference caused by SUs [4]–[6]. In these systems, the status of PUs' activities (i.e., whether or not PUs are busy or idle) and the duration of spectrum sensing affect the system performance [5]–[9]. Spectrum sensing is prone to errors. These errors can be characterized in terms of mis-detection and false alarm probabilities and need to be considered in the system design. Another important factor that impacts the performance of opportunistic CR systems is the level of assumption made regarding the availability of CSI. In opportunistic CR systems, although CSI corresponding to SU-PU link is not required, still CSI corresponding to SU transmitter–SU receiver ($\mathrm{SU_{tx}}$–$\mathrm{SU_{rx}}$) link is needed for properly adapting the data transmission.

In addition to spectral efficiency, energy efficiency is another important metric to consider when designing communication systems [10]–[16]. Energy harvesting (EH) has been recognized as an effective approach for improving the energy efficiency. EH-powered devices can operate without the need for external power cables or periodic battery replacements [17], [18]. EH-enabled CR systems have received substantial attention as a promising solution for increasing both energy efficiency and spectral efficiency [19]–[21]. EH-enabled communication systems can harvest energy from ambient energy sources (e.g., solar, wind, thermal, vibration) or radio frequency (RF) signals. For instance, in an ambient RF EH-enabled CR system, the energy of emitted RF signals from TV/radio broadcast towers, cellular base stations, and Wi-Fi access points (APs) is captured by $\mathrm{SU_{tx}}$ antenna and stored in its battery [22]–[26]. A dedicated RF signal source can be utilized for energy harvesting and enabling simultaneous wireless information and power transfer (SWIPT) [27], [28].

Manuscript received January 30, 2021; revised May 6, 2021; accepted June 2, 2021. Date of publication June 7, 2021; date of current version November 22, 2021. This work was supported by National Science Foundation under Grant CISE-CNS-2006683. The editor coordinating the review of this article was H. Tabassum. *(Corresponding author: Hassan Yazdani.)*

The authors are with the Department of Electrical and Computer Engineering, University of Central Florida, Orlando, FL 32816 USA (e-mail: h.yazdani@knights.ucf.edu; azadeh@ucf.edu).

Digital Object Identifier 10.1109/TGCN.2021.3087456

The body of research on EH-enabled communication systems can be grouped into two main categories, depending on the adopted energy arrival model [10], [29]: in the first model, the energy arrival is deterministic and the transmitter has a causal or non-causal knowledge of the energy arrival at the beginning of transmission [30]. In the second model, the energy arrival is stochastic [10]. In practice, the energy arrival of ambient energy sources, including ambient RF signal sources, is intrinsically time-variant and often sporadic. This natural factor degrades the performance of the battery-free EH-enabled communication systems in which a "harvest-then-transmit" strategy is adopted, i.e., users can only transmit when the energy harvested in one time slot is sufficient for data transmission [31]. To flatten the randomness of the energy arrival, the harvested energy is stored in a battery, to balance the energy arrival and the energy consumption [10]. In practice, the capacity of the batteries is limited, and this can result in an energy overflow.

Power/energy management in EH-enabled communication systems with finite size batteries is necessary, in order to adapt the rate of energy consumption with the rate of energy harvesting. If the energy management policy is overly aggressive, such that the rate of energy consumption is greater than the rate of energy harvesting, the transmitter may stop functioning, due to energy outage. On the other hand, if the energy management policy is overly conservative, the transmitter may fail to utilize the excess energy, due to energy overflow, and the data transmission would become limited in each energy allocation interval.

Focusing on opportunistic EH-enabled CR systems, we realize that power control strategies, aiming at optimizing the performance of SUs, should be designed such that spectrum sensing and its corresponding errors, as well as spectrum sensing-data transmission trade-offs are incorporated in the design process. For instance, the authors in [22] considered a system model, where $\mathrm{SU_{tx}}$ can perform energy harvesting and spectrum sensing simultaneously. Depending on the outcome of its spectrum sensing, $\mathrm{SU_{tx}}$ continues to harvest energy when the spectrum is sensed busy, or transmits data when the spectrum is sensed idle, and studied maximizing $\mathrm{SU_{tx}}$–$\mathrm{SU_{rx}}$ channel capacity, via optimizing the threshold of the energy detector employed for spectrum sensing. Aiming at a similar goal (i.e., maximizing the SU's channel capacity), the authors in [26] considered a modified system model, where $\mathrm{SU_{tx}}$ cannot perform energy harvesting and spectrum sensing at the same time. The authors investigated the optimal mode selection policy (i.e., to choose whether to access the spectrum or to harvest energy) for CR sensor networks. Targeting the same goal as [22], [26], the authors in [7], [16] studied the optimal allocation of energy to be consumed for spectrum sensing versus data transmission, assuming that $\mathrm{SU_{tx}}$ has a finite size data buffer. The authors in [8] considered a different system model, where energy harvesting, spectrum sensing, and data transmission occur in three non-overlapping time intervals within a frame. They studied maximizing the $\mathrm{SU_{tx}}$–$\mathrm{SU_{rx}}$ link throughput, via optimizing the duration of spectrum sensing and the threshold of the energy detector employed for spectrum sensing, and investigated the energy harvesting-spectrum sensing-data transmission trade-offs. We note that the works in [7], [8], [16], [22], [26] assume that CSI of $\mathrm{SU_{tx}}$–$\mathrm{SU_{rx}}$ link is perfectly known at both $\mathrm{SU_{tx}}$ and $\mathrm{SU_{rx}}$.

In general, the power control strategies designed for opportunistic EH-enabled CR systems should depend on the level of assumption made regarding the availability of CSI corresponding to $\mathrm{SU_{tx}}$–$\mathrm{SU_{rx}}$ link, and whether the adapted transmit power levels are continuous or discrete values. In practice, only partial CSI can be available at $\mathrm{SU_{tx}}$ and $\mathrm{SU_{rx}}$ due to several factors (e.g., channel estimation error and limitation of feedback channel from $\mathrm{SU_{rx}}$ to $\mathrm{SU_{tx}}$). Partial CSI has deteriorating effects on the performance of communication systems, including EH-enabled CR systems, and should not be overlooked. In the following, we reference several works that consider the effects of partial CSI on the performance of EH-enabled communication systems, with stochastic energy arrival model and finite size batteries. Assuming perfect CSI at the receiver (Rx) and quantized CSI (due to limited feedback channel) at the transmitter (Tx), the authors in [32] aimed at maximizing the Tx's bit rate, via adapting discrete-valued data transmit power and modulation order, according to the quantized CSI of Tx–Rx link and the Tx battery state. Assuming perfect CSI at the Rx and single-bit partial CSI at the Tx (due to severely limited feedback channel), the authors in [30] targeted at maximizing the Tx-Rx link throughput, via optimizing the threshold of the binary channel quantizer and discrete-valued data transmit power. Assuming perfect CSI at the Rx and partial CSI at the Tx (due to channel estimation error), the authors in [29], [33] analyzed maximizing the Tx's average throughput, in two asymptotic regimes, where the rate of energy harvesting is very small or very large, via optimizing continuous-valued data transmit power. We note that, none of the referenced works in [29], [30], [32], [33] considered CR systems. Furthermore, these works assume that CSI is perfectly known at the Rx.

B. Knowledge Gap and Our Contributions

We consider an uplink opportunistic EH-enabled CR network operating in frequency division duplexing (FDD) mode and, consisting of N_{u} SUs and an access point (AP), that can access a wideband spectrum licensed to a primary network. Each SU is capable of harvesting energy from natural ambient energy sources, and is equipped with a finite size rechargeable battery, to store the harvested energy. Our main *objectives* are 1) to study how the achievable uplink sum-rate of SUs is impacted by the *combined effects* of spectrum sensing error and imperfect CSI of SUs–AP links (due to channel estimation error) and 2) to design an energy management strategy that maximizes the achievable uplink sum-rate of SUs, subject to a constraint on the average interference power that SUs can impose on the PU. To the best of our knowledge, our work is the first to study the impact of these combined effects on the performance of an uplink opportunistic EH-enabled CR network.

The importance of our study is evident by the works in [34]–[39], which demonstrate the significance of considering the effect of imperfect CSI at the Rx, due to channel

estimation, on the Tx achievable rate. We note that the Tx in these works is a primary transmitter (i.e., it is not a secondary transmitter in a CR system) and has a traditional stable power supply. One expects that spectrum sensing error, combined with random energy arrival at the Tx, exacerbates the effect of imperfect CSI on the Tx achievable rate. The challenges of our study are twofold: first, it requires integration of energy harvesting, spectrum sensing, and channel estimation. Successful achievement of this integration entails stochastic modeling of energy arrival, energy storage, and PU's activities. These stochastic models are utilized to establish an achievable sum-rate of SUs that takes into account both spectrum sensing error and channel estimation error. Second, one needs to properly design energy control strategies for SUs, that strike a balance between the energy harvesting and the energy consumption, and adapt transmit power according to the available CSI and the battery state.

We assume that SUs operate under a time-slotted scheme, and SU_n is capable of harvesting energy during the entire time slot. Each time slot consists of three sub-slots corresponding to (i) spectrum sensing phase, during which SU_n senses the spectrum, (ii) channel probing phase, during which SU_n sends pilot symbols to the AP, when the spectrum is sensed idle, for estimating the fading coefficient corresponding to SU_n–AP link, and (iii) data transmission phase, during which SU_n sends data symbols to the AP. Assuming that the AP feeds back its estimate of the fading coefficient to SU_n, SU_n adapts its transmit power based on this information as well as the available energy in its battery.

Our main contributions can be summarized as follow:

1) Our system model encompasses the stochastic energy arrival model for harvesting energy, the stochastic energy storage model for the finite size battery, the stochastic model of PU's activities, spectrum sensing error, and channel estimation error at both SUs and the AP. We model the dynamics of the battery as a finite state Markov chain.

2) We propose a power adaptation strategy for SU_n that mimics the behavior of the rate-optimal power adaptation scheme with respect to the estimated channel power gain $\widehat{g}_n$ available at SU_n and the AP, i.e., when $\widehat{g}_n$ is below a cut-off threshold θ_n, the transmit energy is zero, and when $\widehat{g}_n$ exceeds θ_n, the transmit energy increases monotonically in proportion to a parameter Ω_n, as $\widehat{g}_n$ increases. The parameters Ω_n and θ_n play key roles in balancing the energy harvesting and the energy consumption.

3) Given our system model, we establish a lower bound on the achievable uplink sum-rate of SUs-AP links, in the presence of both spectrum sensing error and channel estimation error at both SUs and the AP. We formulate a novel constrained optimization problem with the optimization variables $\{\Omega_n, \theta_n\}_{n=1}^{N_\mathrm{u}}$, aiming at maximizing the derived uplink sum-rate lower bound, subject to the average interference constraint (AIC) imposed on the PU and the causality constraint of the battery. We solve the formulated constrained optimization problem assuming that the battery reaches its steady-state.

4) We derive closed form expressions for the battery outage probability and transmission outage probability and demonstrate their behaviors, in terms of the average number of harvesting energy packets and the AIC. We also study the existing trade-offs between spectrum sensing-channel probing-data transmission and how these trade-offs impact the uplink sum-rate of our CR network.

Our work is different from [29]–[32]. In particular, these works view the energy management policy design as a sequential decision making problem, and hence, they adopt the Markov decision process (MDP) framework to solve the problem. In this framework, the goal is typically optimizing a specific metric over a horizon spanning several time slots. The obtained solutions using dynamic programming are dependent across time slots, and also depend on the initial condition (i.e., the initial state of the battery). Here, we assume that the battery operates at its steady-state, and hence, our proposed constrained optimization problem can be solved for each time slot. Furthermore, the problem can be solved *offline* and the optimized transmission parameters $\{\Omega_n, \theta_n\}_{n=1}^{N_\mathrm{u}}$, which do *not* depend on the initial condition of the battery, can become available *apriori* at the AP and SUs. During the data transmission phase, SU_n chooses its symbol power, using its optimized transmission parameters Ω_n, θ_n, and based on its partial CSI of SU_n-AP link received via the feedback channel as well as the available energy in its battery.

C. Paper Organization

The remainder of the paper is organized as follows. Section II explains our system model. Section III describes the spectrum sensing phase and our binary energy-based detector for detecting PU activity. Section IV discusses the channel probing phase. Section V explains the data transmission phase and derives a lower bound on the achievable uplink sum-rate of our CR network. Also, it formulates our proposed constrained optimization problem. Section VI corroborates our analysis on the proposed optimization problem with MATLAB simulations. Section VII concludes the paper.

II. System Model

We consider an uplink opportunistic EH-enabled CR network, operating in FDD mode, that can access a wideband spectrum band licensed to a primary network, consisting of *M* non-overlapping narrowband spectrum bands, each with a bandwidth of *W* Hz [3]. The primary network consists of a primary transmitter (PU_tx) and a primary receiver (PU_rx). The secondary network consists of an AP and N_u SUs (see Fig. 1). The AP can serve up to *M* SUs simultaneously and we assume that $N_\mathrm{u} \leq M$. We also assume that narrowband spectrum bands are pre-assigned to SUs and thus each SU knows which band to sense and transmit data over. The SUs are equipped with identical energy harvesting circuits to harvest energy from the ambient environment and identical finite size batteries for energy storage (see Fig. 2). We consider block fading channel model and suppose flat fading coefficients from PU_tx to SU_n, PU_tx to AP, SU_n to PU_rx, and, SU_n to AP are four independent zero-mean complex Gaussian random variables, which we denote by u_n, q, z_n and h_n with variances δ_{u_n}, δ_q, δ_{z_n} and γ_n, respectively.

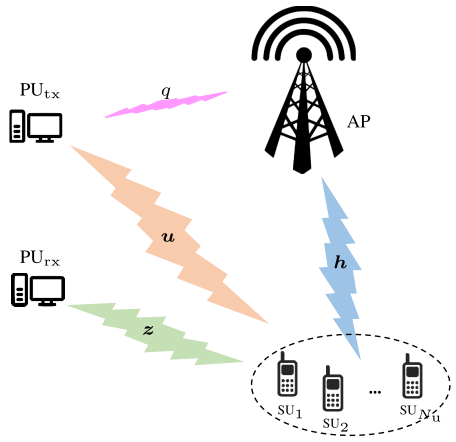

Fig. 1. Schematics of the uplink CR network.

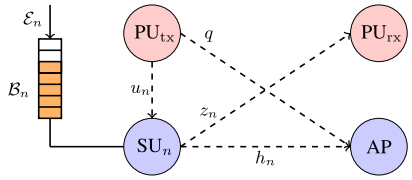

Fig. 2. Our CR system model corresponding to SU$_n$ for $n = 1, \ldots, N_{\rm u}$.

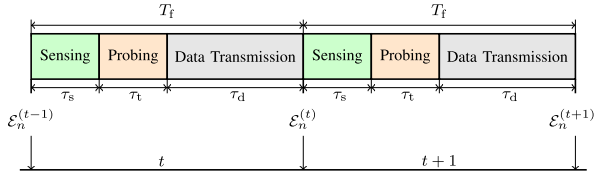

Fig. 3. Slot structure of SUs.

A. Battery and Energy Harvesting Models

We assume that SUs operate under a time-slotted scheme, with slot duration of $T_{\rm f}$ seconds, and they always have data to transmit. Each time slot is indexed by an integer t for $t = 1, 2, \ldots$ The energy harvester at each SU stores randomly arriving energy packets in a finite size battery and consumes the stored (harvested) energy for spectrum sensing, channel probing, and data transmission. Each battery consists of K cells (units) and the amount of energy stored in each unit is equal to $e_{\rm u}$ Joules. Thus, the battery can store up to $Ke_{\rm u}$ Joules of energy.

When k cells of the battery is charged (i.e., the amount of stored energy in the battery is $ke_{\rm u}$ Joules) we say that the battery *is at state* k. Let $\mathcal{B}_n^{(t)} \in \{0, 1, \ldots, K\}$ denote the discrete random process indicating the battery state of SU$_n$ at the beginning of time slot t. We define the probability mass function (pmf) of the discrete random variable $\mathcal{B}_n^{(t)}$ as $\zeta_{k,n}^{(t)} = \Pr(\mathcal{B}_n^{(t)} = k)$, where $\sum_{k=0}^{K} \zeta_{k,n}^{(t)} = 1$. Note that $\mathcal{B}_n^{(t)} = 0$ and $\mathcal{B}_n^{(t)} = K$ represent the empty battery and full battery levels, respectively.

Let $\mathcal{E}_n^{(t)}$ denote the randomly arriving energy packets at SU$_n$ during time slot t, where the energy packet measured in Joules is e_u Joules. The discrete random process $\mathcal{E}_n^{(t)}$ is typically modeled as a sequence of independent and identically distributed (i.i.d.) random variables [16], regardless of the spectrum occupancy state of PU$_{\rm tx}$. We assume that the discrete random variables $\mathcal{E}_n^{(t)}$'s are i.i.d. over time and independent across sensors. We model $\mathcal{E}_n^{(t)}$ as a Poisson random variable with the pmf $f_{\mathcal{E}_n}(r) = \Pr(\mathcal{E} = r) = e^{-\rho_n}\rho_n^r/r!$ for $r = 0, 1, \ldots, \infty$, where ρ_n denotes the average number of arriving energy packets during one time slot of SU$_n$.[1] Let $\alpha_{h_n}^{(t)}$ be the number of stored (harvested) energy units in the battery at SU$_n$ during time slot t. This harvested energy $\alpha_{h_n}^{(t)}$ cannot be used during time slot t. Since the battery has a finite capacity of K cells, we find that $\alpha_{h_n}^{(t)}$ is an element of the finite set $\{0, 1, \ldots, K\}$. Also, $\alpha_{h_n}^{(t)}$ are i.i.d. over time slots and independent across sensors. Let $f_{\alpha_{h_n}}(r) = \Pr(\alpha_{h_n} = r)$ denote the pmf of $\alpha_{h_n}^{(t)}$. We can find the pmf of $\alpha_{h_n}^{(t)}$ in terms of the pmf of $\mathcal{E}_n^{(t)}$ as the following[2]

$$f_{\alpha_{h_n}}(r) = \begin{cases} f_{\mathcal{E}_n}(r), & \text{if } 0 \le r \le K-1 \\ \sum_{m=K}^{\infty} f_{\mathcal{E}_n}(m), & \text{if } r = K. \end{cases} \quad (1)$$

B. Slot Structure of SUs

Each time slot consists of three sub-slots (see Fig. 3), corresponding to spectrum sensing phase, channel probing phase, and data transmission phase, with fixed durations of $\tau_{\rm s} = N_{\rm s}/f_{\rm s}, \tau_{\rm t} = N_{\rm t}/f_{\rm s}, \tau_{\rm d} = N_{\rm d}/f_{\rm s}$, respectively. Note that $f_{\rm s}$ is the sampling frequency, $N_{\rm s}$ is the number of collected samples during spectrum sensing phase, $N_{\rm t}$ is the number of training symbols sent during channel probing phase, and $N_{\rm d}$ is the number of data symbols sent during data transmission phase. Also, we have $T_{\rm f} = \tau_{\rm s} + \tau_{\rm t} + \tau_{\rm d}$.

During *spectrum sensing phase*, SU$_n$ senses its pre-assigned single spectrum band to detect PU$_{\rm tx}$'s activity. We model the PU$_{\rm tx}$'s activity in each spectrum band as a Bernoulli random variable and we assume the statistics of PU$_{\rm tx}$ are i.i.d. across M spectrum bands and over time slots. Therefore, we can frame the spectrum sensing problem at SU$_n$ as a binary hypothesis testing problem. Suppose $\mathcal{H}_1^{(t)}$ and $\mathcal{H}_0^{(t)}$ represent the binary hypotheses of PU$_{\rm tx}$ being active and inactive in time slot t, respectively, with prior probabilities $\Pr\{\mathcal{H}_1^{(t)}\} = \pi_1$ and $\Pr\{\mathcal{H}_0^{(t)}\} = \pi_0$. SU$_n$ applies a binary detection rule to decide whether or not PU$_{\rm tx}$ is active in its pre-assigned band. Let $\widehat{\mathcal{H}}_{0,n}$ and $\widehat{\mathcal{H}}_{1,n}$, with probabilities $\widehat{\pi}_{0,n} = \Pr\{\widehat{\mathcal{H}}_{0,n}\}$ and $\widehat{\pi}_{1,n} = \Pr\{\widehat{\mathcal{H}}_{1,n}\}$, denote the SU$_n$ detector outcome, i.e., the detector finds PU$_{\rm tx}$ active and inactive (i.e., the result of spectrum sensing is busy or idle), respectively. The accuracy

[1] We note that ρ_n does not depend on the duration of spectrum sensing phase, since we assume each node is capable of harvesting energy during the entire slot. If we limit harvesting energy to spectrum sensing phase, then ρ_n would change to $\rho_n \tau_{\rm s}/T_{\rm f}$. Poisson distribution for statistical modeling of ambient energy and solar energy has been applied before in [40]. We note, however, that our analysis is not tied to this specific distribution and can be applied for any discrete non-Poisson distribution.

[2] Equation (1) assumes that the energy storage process is lossless. For a lossy storage process, one needs to model such loss via establishing a functional relationship between α_{h_n} and $\mathcal{E}_n$, i.e., $\alpha_{h_n} = J_n(\mathcal{E}_n)$, where the function $J_n(\cdot)$ can be approximated using the battery type and specifications. Knowing $J_n(\cdot)$ and the pmf $f_{\mathcal{E}_n}(r)$, one can find the pmf $f_{\alpha_{h_n}}(r)$ using transformation method.

of this binary detector is characterized by its false alarm and detection probabilities. The details of the binary detector are presented in Section III.

Depending on the outcome of its spectrum sensing, SU_n stays in spectrum sensing phase or enters *channel probing phase*. In channel probing phase, SU_n sends N_t training symbols with fixed symbol power $P_\mathrm{t} = \alpha_\mathrm{t} e_\mathrm{u}/\tau_\mathrm{t}$, to enable channel estimation at the AP, where α_t is the number of consumed cells of energy for channel probing.[3] We assume that the battery always has α_t units of stored energy for channel probing. Let $h_n^{(t)}$ denote the SU_n-AP fading coefficient in time slot t and $g_n^{(t)} = |h_n^{(t)}|^2$ be the corresponding channel power gain. Using the received signals corresponding to the training symbols, the AP estimates $\widehat{h}_n^{(t)}$ and lets $\widehat{g}_n^{(t)} = |\widehat{h}_n^{(t)}|^2$ and shares this value with SU_n via a feedback channel. Next, SU_n enters *data transmission phase*. During this phase, SU_n sends N_d Gaussian data symbols with adaptive symbol power according to its battery state and the received information via the feedback channel about SU_n–AP link. When the battery is at state k and the feedback information is $\widehat{g}_n^{(t)}$, then SU_n allocates $\alpha_{k,n}^{(t)}$ cells of its stored energy for each data symbol transmission, implying that the adaptive symbol power is $P_{k,n}^{(t)} = \alpha_{k,n}^{(t)} p_\mathrm{u}$, where $p_\mathrm{u} = e_\mathrm{u}/\tau_\mathrm{d}$. Note that since $\alpha_{k,n}^{(t)}$ is discrete, $P_{k,n}^{(t)}$ is discrete. The details of the choice of $\alpha_{k,n}^{(t)}$ according to the battery state k and the feedback information $\widehat{g}_n^{(t)}$ are given in Section II-C and the details of channel estimation are explained in Section IV.

C. Transmission Model and Battery Dynamics

As we stated, we assume that during time slot t SU_n adapts its transmit energy per data symbol (transmit power) according to its battery state k and the feedback information $\widehat{g}_n^{(t)}$. In particular, we choose a power adaptation strategy that mimics the behavior of the rate-optimal power adaptation scheme with respect to the channel power gain [6], i.e., when $\widehat{g}_n^{(t)}$ is smaller than a cut-off threshold θ_n (to be optimized), the transmit energy is zero, and when $\widehat{g}_n^{(t)}$ exceeds θ_n, the transmit energy increases monotonically as $\widehat{g}_n^{(t)}$ increases until it reaches its maximum value of $\lfloor k\Omega_n \rfloor - \alpha_\mathrm{t}$, where $\Omega_n \in [0,1]$ (to be optimized), and $\lfloor \cdot \rfloor$ denotes the floor function. Mathematically, we express $\alpha_{k,n}^{(t)}$ for SU_n as the following

$$\alpha_{k,n}^{(t)} = \max\left\{\overline{\alpha}_{k,n}^{(t)}, 0\right\}, \quad \text{for } k = 0, 1, \ldots, K, \tag{2a}$$

$$\overline{\alpha}_{k,n}^{(t)} = \left\lfloor \Omega_n k \left(1 - \frac{\theta_n}{\widehat{g}_n^{(t)}}\right)^+ \right\rfloor - \alpha_\mathrm{t}, \tag{2b}$$

where $(x)^+ = \max\{x, 0\}$. The parameters Ω_n and θ_n in (2) play key roles in balancing the energy harvesting and the energy consumption for transmission. Given θ_n, when Ω_n is large (or given Ω_n, when θ_n is small), such that the rate of energy consumption for transmission is greater than the rate of energy harvesting, SU_n may stop functioning, due to energy outage. On the other hand, given θ_n, when Ω_n is small (or given Ω_n, when θ_n is large), SU_n may fail to utilize the excess energy, due to energy overflow, and the data transmission would become limited in each time slot. Note that $\overline{\alpha}_{k,n}^{(t)}$ in (2) ensures that the battery always has α_t units of stored energy for channel probing. Furthermore, the transmission policy in (2) satisfies the causality constraint of the battery. The causality constraint restrains the energy corresponding to symbol transmit power to be less than the available stored energy in the battery, i.e., $\alpha_{k,n}^{(t)} \le k - \alpha_\mathrm{t}$. Note that $\alpha_{k,n}^{(t)}$ is a discrete random variable and $\alpha_{k,n}^{(t)} \in \{0, 1, \ldots, K - \alpha_\mathrm{t}\}$.[4] Let $\psi_{i,k,n}^{\varepsilon} = \Pr(\alpha_{k,n}^{(t)} = i | \mathcal{H}_\varepsilon)$ denote the conditional pmf of $\alpha_{k,n}^{(t)}$ given $\mathcal{H}_\varepsilon, \varepsilon = 0, 1$. We have

$$\psi_{i,k,n}^{\varepsilon} = \begin{cases} 1, & \text{if} \quad 0 \le k \le \alpha_\mathrm{t},\ i = 0 \\ 0, & \text{if} \quad 0 \le k \le \alpha_\mathrm{t},\ i \ne 0 \\ Y_{k,n}^{\varepsilon}, & \text{if} \quad k \ge \alpha_\mathrm{t} + !1,\ i = 0 \\ Q_{i,k,n}^{\varepsilon}, & \text{if} \quad k \ge \alpha_\mathrm{t} + 1,\ 1 \le i \le \lfloor k\Omega_n \rfloor - \alpha_\mathrm{t} \\ 0, & \text{if} \quad k \ge \alpha_\mathrm{t} + 1,\ i \ge \lfloor k\Omega_n \rfloor - \alpha_\mathrm{t} + 1 \end{cases} \tag{3}$$

in which

$$Q_{i,k,n}^{\varepsilon} = F_{\widehat{g}_n}^{\varepsilon}\left(c_{i,k,n}\right) - F_{\widehat{g}_n}^{\varepsilon}\left(a_{i,k,n}\right) \tag{4a}$$

$$Y_{k,n}^{\varepsilon} = F_{\widehat{g}_n}^{\varepsilon}(\theta_n) + \sum_{m=1}^{\min(\lfloor k\Omega_n \rfloor, \alpha_\mathrm{t})} Q_{m-\alpha_\mathrm{t},k,n}^{\varepsilon} \tag{4b}$$

$$a_{i,k,n} = \frac{\theta_n k \Omega_n}{k\Omega_n - \alpha_\mathrm{t} - i}, \quad c_{i,k,n} = \frac{\theta_n k \Omega_n}{k\Omega_n - \alpha_\mathrm{t} - i - 1}, \tag{4c}$$

where $F_{\widehat{g}_n}^{\varepsilon}(x) = F_{\widehat{g}_n}(x|\mathcal{H}_\varepsilon)$ is the cumulative distribution function (CDF) of $\widehat{g}_n$ given $\mathcal{H}_\varepsilon$. Note that if $c_{i,k,n} < 0$, we set $c_{i,k,n} = +\infty$.

The battery state at the beginning of time slot $t+1$ depends on the battery state at the beginning of time slot t, the harvested energy during time slot t, the transmission symbol, as well as α_t. In particular, if at time slot t, SU_n senses its spectrum band to be idle, the state of its battery at the beginning of slot $t+1$ is

$$\mathcal{B}_n^{(t+1)} = \min\left\{\left(\mathcal{B}_n^{(t)} - \alpha_\mathrm{t} - \alpha_{k,n}^{(t)} + \alpha_{h_n}^{(t)}\right)^+, K\right\}. \tag{5}$$

On the other hand if at time slot t, SU_n senses its spectrum band to be busy, the state of its battery at the beginning of slot $t+1$ is

$$\mathcal{B}_n^{(t+1)} = \min\left\{\left(\mathcal{B}_n^{(t)} + \alpha_{h_n}^{(t)}\right)^+, K\right\}, \tag{6}$$

since $\alpha_{k,n}^{(t)} = 0$. Considering the dynamic battery state model in (5) and (6) we note that, conditioned on $\alpha_{h_n}^{(t)}$ and $\alpha_{k,n}^{(t)}$ the

[3]For ease of presentation, we assume that circuit power (energy) consumption is negligible in comparison to the consumed energy for channel probing and data transmission. Otherwise, it can easily be incorporated into the system model.

[4]Examining (2) we realize that the largest value that $\alpha_{k,n}^{(t)}$ can take is $K - \alpha_\mathrm{t}$. Hence, the maximum transmit energy of SU_n is bounded by $K - \alpha_\mathrm{t}$. The system designer can choose K such that signal distortion, due to the nonlinear behavior of power amplifiers, is prevented and the operation of power amplifiers in their linear regions is guaranteed.

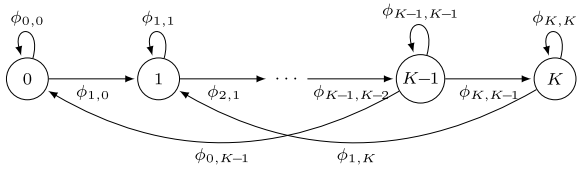

Fig. 4. Schematics of Markov chain corresponding to the battery state random process $\mathcal{B}_n^{(t)}$.

value of $\mathcal{B}_n^{(t+1)}$ only depends on the value of $\mathcal{B}_n^{(t)}$ (and not the battery states of time slots before t). Hence, the battery state random process $\mathcal{B}_n^{(t)}$ can be modeled as a Markov chain (see Fig. 4). Let the probability vector of battery state in time slot t be $\boldsymbol{\zeta}_n^{(t)} = [\zeta_{1,n}^{(t)}, \ldots, \zeta_{K,n}^{(t)}]^T$. Note that the probability $\zeta_{k,n}^{(t)}$ depends on the battery state at slot $t-1$, the number of battery units filled by the harvested energy during slot $t-1$, the probability of spectrum band sensed idle, and, the number of energy units allocated for data transmission at slot $t-1$ when the spectrum band is sensed idle, i.e., $\zeta_{k,n}^{(t)}$ depends on $\mathcal{B}_n^{(t-1)}, \alpha_{h_n}^{(t-1)}, \widehat{\pi}_{0,n}, \alpha_{k,n}^{(t-1)}$, respectively. Assuming the Markov chain is time-homogeneous,[5] we let $\boldsymbol{\Phi}_n$ denote the $(K+1)\times(K+1)$ transition probability matrix of this chain with its $(i+1, j+1)$-th entry $\phi_{i,j}^n = \Pr(\mathcal{B}_n^{(t)} = i | \mathcal{B}_n^{(t-1)} = j)$ given in (7), shown at the bottom of the page, where $F_{\alpha_{h_n}}(\cdot)$ is the commutative distribution function (CDF) of α_{h_n}. We have

$$\boldsymbol{\zeta}_n^{(t+1)} = \boldsymbol{\Phi}_n \boldsymbol{\zeta}_n^{(t)}. \tag{8}$$

Since the Markov chain characterized by the transition probability matrix $\boldsymbol{\Phi}_n$ is irreducible and aperiodic, there exists a unique steady-state distribution, regardless of the initial state [41]. Let $\boldsymbol{\zeta}_n = \lim_{t\to\infty} \boldsymbol{\zeta}_n^{(t)}$ be the unique steady-state probability vector. This vector satisfies the following equations

$$\boldsymbol{\zeta}_n = \boldsymbol{\Phi}_n \boldsymbol{\zeta}_n, \tag{9a}$$

$$\boldsymbol{\zeta}_n^T \mathbf{1} = \sum_{k=1}^{K} \zeta_{k,n} = 1, \tag{9b}$$

where $\mathbf{1}$ is an all-ones vector, i.e., $\boldsymbol{\zeta}_n$ is the normalized eigenvector corresponding to the unit eigenvalue of $\boldsymbol{\Phi}_n$, such that the entries of $\boldsymbol{\zeta}_n$ sums up to one. The closed-form expression for $\boldsymbol{\zeta}_n$ is [42]

$$\boldsymbol{\zeta}_n = (\boldsymbol{\Phi}_n - \boldsymbol{I} + \boldsymbol{B})^{-1}\mathbf{1}, \tag{10}$$

where $\boldsymbol{B}$ is an all-ones matrix and $\boldsymbol{I}$ is the identity matrix. From this point forward, we assume that the battery is at its steady-state and we drop the superscript t.

To illustrate our symbol transmission model in (2) we consider the following simple numerical example. Assuming that the battery has $K = 7$ cells, Fig. 5 shows an example of $\alpha_{k,n}$ for our CR system for two sets of $\{\Omega_n, \theta_n\}$ given as $\Omega_n^{(a)} = 0.75, \theta_n^{(a)} = 0.02$ and $\Omega_n^{(b)} = 0.95, \theta_n^{(b)} = 0.02$. The corresponding transition probability matrices are given in the following

$$\boldsymbol{\Phi}_n^{(a)} = \begin{pmatrix} 0.42 & 0.29 & 0.17 & 0.08 & 0.02 & 0 & 0 & 0 \\ 0.12 & 0.13 & 0.12 & 0.09 & 0.05 & 0.02 & 0 & 0 \\ 0.19 & 0.12 & 0.13 & 0.12 & 0.09 & 0.05 & 0.02 & 0 \\ 0.07 & 0.19 & 0.12 & 0.13 & 0.12 & 0.09 & 0.05 & 0.02 \\ 0.05 & 0.07 & 0.19 & 0.12 & 0.13 & 0.12 & 0.09 & 0.05 \\ 0.05 & 0.05 & 0.07 & 0.19 & 0.12 & 0.13 & 0.12 & 0.09 \\ 0.04 & 0.05 & 0.05 & 0.07 & 0.19 & 0.12 & 0.13 & 0.12 \\ 0.06 & 0.1 & 0.15 & 0.2 & 0.27 & 0.46 & 0.58 & 0.71 \end{pmatrix},$$

$$\boldsymbol{\Phi}_n^{(b)} = \begin{pmatrix} 0.54 & 0.43 & 0.31 & 0.18 & 0.08 & 0.03 & 0 & 0 \\ 0.18 & 0.11 & 0.13 & 0.12 & 0.1 & 0.06 & 0.02 & 0 \\ 0.04 & 0.18 & 0.11 & 0.13 & 0.12 & 0.1 & 0.06 & 0.02 \\ 0.04 & 0.04 & 0.18 & 0.11 & 0.13 & 0.12 & 0.1 & 0.06 \\ 0.05 & 0.04 & 0.04 & 0.18 & 0.11 & 0.13 & 0.12 & 0.1 \\ 0.05 & 0.05 & 0.04 & 0.04 & 0.18 & 0.11 & 0.13 & 0.12 \\ 0.04 & 0.05 & 0.05 & 0.04 & 0.04 & 0.18 & 0.11 & 0.13 \\ 0.06 & 0.1 & 0.15 & 0.2 & 0.24 & 0.28 & 0.46 & 0.57 \end{pmatrix}.$$

TABLE I
MOST COMMONLY USED SYMBOLS

Symbol	Description
N_s	Number of collected samples during *spectrum sensing phase*
N_t	Number of training symbols during *channel probing phase*
N_d	Number of data symbols during *data transmission phase*
P_t	Power of training symbols
$h_n, \widehat{h}_n, \widetilde{h}_n$	Fading coefficient of SU_n–AP link, LMMSE channel estimate, and its corresponding estimation error
$\gamma_n, \widehat{\gamma}_n, \widetilde{\gamma}_n$	Variances of $h_n, \widehat{h}_n, \widetilde{h}_n$
π_0, π_1	Prior probabilities of $\mathcal{H}_0$ and $\mathcal{H}_1$
$\widehat{\pi}_{0,n}, \widehat{\pi}_{1,n}$	Probabilities of spectrum bands being sensed idle or busy
$\zeta_{k,n}$	Probability of SU_n battery being at state k
u_n	Fading coefficient of PU_tx–SU_n link with variance δ_{u_n}
q	Fading coefficient of PU_tx–AP link with variance δ_q
z_n	Fading coefficient of SU_n–PU_rx link with variance δ_{z_n}

[5]A Markov chain is time-homogeneous (stationary) if and only if its transition probability matrix is time-invariant. Adopting homogeneous Markov chain model for studying EH-enabled communication systems is widely common [41].

$$\phi_{0,j}^n = \sum_{l=0}^{K} \Big[\psi_{l,j,n}^0 \widehat{\pi}_{0,n} F_{\alpha_{h_n}}(\alpha_\mathrm{t} + l - j)\Big] + \widehat{\pi}_{1,n} F_{\alpha_{h_n}}(-j) \tag{7a}$$

$$\phi_{K,j}^n = \sum_{l=0}^{K} \Big[\psi_{l,j,n}^0 \widehat{\pi}_{0,n} \big(1 - F_{\alpha_{h_n}}(\alpha_\mathrm{t} + l + K - j)\big)\Big] + \widehat{\pi}_{1,n} \big(1 - F_{\alpha_{h_n}}(K - j)\big) \tag{7b}$$

$$\phi_{i,j}^n = \sum_{l=0}^{K} \Big[\psi_{l,j,n}^0 \widehat{\pi}_{0,n} f_{\alpha_{h_n}}(\alpha_\mathrm{t} + l + i - j)\Big] + \widehat{\pi}_{1,n} f_{\alpha_{h_n}}(i - j), \qquad \text{for } i = 1, \ldots, K-1 \tag{7c}$$

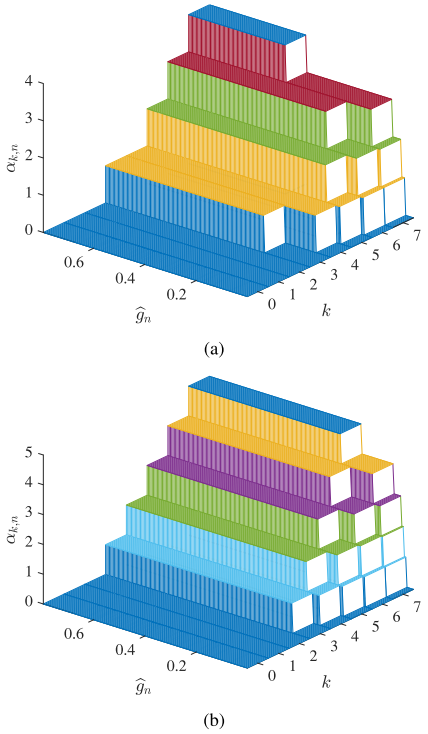

Fig. 5. This example shows how many energy units ($\alpha_{k,n}$) SU_n spends for data transmission, given its battery state and the received information about its channel gain via feedback link. (a) $\Omega_n^{(a)} = 0.75, \theta_n^{(a)} = 0.02$, (b) $\Omega_n^{(b)} = 0.95, \theta_n^{(b)} = 0.02$.

Our goal is to find the transmission parameters $\{\Omega_n, \theta_n\}$ in (2b) for all SUs such that the uplink sum-rate of our CR network is maximized, subject to a constraint on the average interference power that collective SUs can impose on PU_{rx}. We assume that this optimization problem is solved *offline* at AP, given the *statistical* information of (i) fading channels and noises, (ii) randomly arriving energy packets, and (iii) PU's activities, the number of samples collected during spectrum sensing phase N_s, the number of training symbols sent during channel probing phase N_t and power of training symbols P_t. The solutions to this optimization problem, i.e., the optimal set $\{\Omega_n, \theta_n\}_{n=1}^{N_\text{u}}$ is available *a priori* at the AP and SUs, to be utilized for adapting symbol power during data transmission phase. The idea of offline power allocation optimization with a limited feedback channel has been used before for distributed detection systems in wireless sensor networks [43]. In the following sections, we describe how SUs operate during spectrum sensing phase, channel probing phase, and data transmission phase. For the readers' convenience, we have collected the most commonly used symbols in Table I.

III. Spectrum Sensing Phase

In order to access its spectrum band, SU_n first needs to sense its band during spectrum sensing phase, to determine whether it is busy or idle (see Fig. 3). We formulate the spectrum sensing at SU_n as a binary hypothesis testing problem, where the received signal at SU_n can be written as:

$$\begin{aligned} \mathcal{H}_0 &: y_n[m] = w_n[m], \\ \mathcal{H}_1 &: y_n[m] = u_n[m]\, p[m] + w_n[m], \end{aligned} \tag{11}$$

for $m = 1, \ldots, N_\text{s}$, where $p[m]$ is the transmit signal of PU_{tx}, $w_n[m] \sim \mathcal{CN}(0, \sigma_{w_n}^2)$ is the additive white Gaussian noise (AWGN) at SU_n and $u_n[m]$ is the fading coefficient corresponding to PU_{tx}–SU_n channel. The two hypotheses $\mathcal{H}_0$ and $\mathcal{H}_1$ with probabilities π_0 and $\pi_1 = 1 - \pi_0$ denote the spectrum is truly idle and truly busy, respectively. We assume that π_0 and π_1 are known to SUs based on long-term spectrum measurements. For spectrum sensing we consider energy detector, where the decision statistics at SU_n is $Z_n = \frac{1}{N_\text{s}} \sum_{m=1}^{N_\text{s}} |y_n[m]|^2$. The accuracy of this detector is characterized by its false alarm probability $P_{\text{fa}_n} = \Pr(\widehat{\mathcal{H}}_{1,n}|\mathcal{H}_0) = \Pr(Z_n > \xi_n|\mathcal{H}_0)$ and detection probability $P_{\text{d}_n} = \Pr(\widehat{\mathcal{H}}_{1,n}|\mathcal{H}_1) = \Pr(Z_n > \xi_n|\mathcal{H}_1)$, where ξ_n is the local decision threshold. For large N_s, we can invoke central limit theorem and approximate the cumulative distribution function (CDF) of Z_n as Guassian. Hence, P_{fa_n} and P_{d_n} can be expressed in terms of Q function as below [44]

$$P_{\text{fa}_n} = Q\left(\left(\frac{\xi_n}{\sigma_{w_n}^2} - 1\right)\sqrt{N_\text{s}}\right), \tag{12a}$$

$$P_{\text{d}_n} = Q\left(\left(\frac{\xi_n}{\sigma_{w_n}^2} - \nu_n - 1\right)\sqrt{\frac{N_\text{s}}{2\nu_n + 1}}\right), \tag{12b}$$

where $\nu_n = P_\text{p}\delta_{u_n}/\sigma_{w_n}^2$ and P_p is the average transmit power of PU_{tx}. For a given value of $P_{\text{d}_n} = \overline{P}_\text{d}$, the false alarm probability can be written as

$$P_{\text{fa}_n} = Q\left(\sqrt{2\nu_n + 1}\, Q^{-1}\left(\overline{P}_\text{d}\right) + \nu_n \sqrt{\tau_\text{s} f_\text{s}}\right). \tag{13}$$

The probabilities $\widehat{\pi}_{0,n}$ and $\widehat{\pi}_{1,n}$ corresponding to the SU_n detector outcome $\widehat{\mathcal{H}}_{0,n}$ and $\widehat{\mathcal{H}}_{1,n}$ respectively, are related to P_{d_n} and P_{fa_n}. In particular, we have $\widehat{\pi}_{0,n} = \beta_{0,n} + \beta_{1,n}$ and $\widehat{\pi}_{1,n} = 1 - \widehat{\pi}_{0,n}$ where

$$\beta_{0,n} = \Pr\left\{\mathcal{H}_0, \widehat{\mathcal{H}}_{0,n}\right\} = \pi_0\left(1 - P_{\text{fa}_n}\right), \tag{14a}$$

$$\beta_{1,n} = \Pr\left\{\mathcal{H}_1, \widehat{\mathcal{H}}_{0,n}\right\} = \pi_1\left(1 - P_{\text{d}_n}\right). \tag{14b}$$

IV. Channel Probing Phase

Depending on the outcome of its spectrum sensing, SU_n either stays in spectrum sensing phase (i.e., remains silent in the remaining of time slot) if its band is sensed busy (i.e., the detector outcome is $\widehat{\mathcal{H}}_{1,n}$), or it enters channel probing phase if its band is sensed idle (i.e., the detector outcome is $\widehat{\mathcal{H}}_{0,n}$). During channel probing phase, we assume SU_n sends training vector $\boldsymbol{x}_t = \sqrt{P_\text{t}}\,\mathbf{1}$, where $\mathbf{1}$ is an $N_\text{t} \times 1$ all-ones vector to enable channel estimation at the AP. Let vector $\boldsymbol{s}_n = [s_n(1), \ldots, s_n(N_\text{t})]^T$ denote the discrete-time representation of received training symbols at the AP from SU_n. Assuming the fading coefficient h_n corresponding to SU_n–AP channel is unchanged during the entire time slot, we have

$$\begin{aligned} \mathcal{H}_0, \widehat{\mathcal{H}}_{0,n} &: s_n[m] = h_n\sqrt{P_\text{t}} + v_n[m], \\ \mathcal{H}_1, \widehat{\mathcal{H}}_{0,n} &: s_n[m] = h_n\sqrt{P_\text{t}} + q[m]p[m] + v_n[m], \end{aligned} \tag{15}$$

for $m = 1, \ldots, N_\text{t}$, $v_n[m] \sim \mathcal{CN}(0, \sigma_{v_n}^2)$ is the AWGN at the AP, and $q[m]$ is the fading coefficient corresponding to PU_{tx}–AP channel. The linear minimum mean square error (LMMSE)

estimate of h_n given $\widehat{\mathcal{H}}_{0,n}$ is [6], [45]

$$\widehat{h}_n = C_{h_n \boldsymbol{s}_n} C_{\boldsymbol{s}_n}^{-1} \boldsymbol{s}_n, \tag{16a}$$

$$C_{h_n \boldsymbol{s}_n} = \mathbb{E}\{h_n \boldsymbol{s}_n^H | \widehat{\mathcal{H}}_{0,n}\} = \gamma_n \sqrt{P_{\mathrm{t}}} \mathbf{1}, \tag{16b}$$

$$C_{\boldsymbol{s}_n} = \mathbb{E}\Big\{ \boldsymbol{s}_n \boldsymbol{s}_n^H | \widehat{\mathcal{H}}_{0,n} \Big\} = \omega_{0,n} \mathbb{E}\Big\{ \boldsymbol{s}_n \boldsymbol{s}_n^H | \mathcal{H}_0, \widehat{\mathcal{H}}_{0,n} \Big\} + \omega_{1,n} \mathbb{E}\Big\{ \boldsymbol{s}_n \boldsymbol{s}_n^H | \mathcal{H}_1, \widehat{\mathcal{H}}_{0,n} \Big\}, \tag{16c}$$

where

$$\omega_{0,n} = \Pr\Big\{ \mathcal{H}_0 | \widehat{\mathcal{H}}_{0,n} \Big\} = \frac{\pi_0 \big(1 - P_{\mathrm{fa}_n}\big)}{\widehat{\pi}_{0,n}} = \frac{\beta_{0,n}}{\widehat{\pi}_{0,n}}, \tag{17a}$$

$$\omega_{1,n} = \Pr\Big\{ \mathcal{H}_1 | \widehat{\mathcal{H}}_{0,n} \Big\} = \frac{\pi_1 \big(1 - P_{\mathrm{d}_n}\big)}{\widehat{\pi}_{0,n}} = \frac{\beta_{1,n}}{\widehat{\pi}_{0,n}}, \tag{17b}$$

and

$$\mathbb{E}\Big\{ \boldsymbol{s}_n \boldsymbol{s}_n^H | \mathcal{H}_0, \widehat{\mathcal{H}}_{0,n} \Big\} = \Big(\widehat{\gamma}_n^0 P_{\mathrm{t}} + \sigma_{v_n}^2 \Big) \boldsymbol{I}, \tag{18a}$$

$$\mathbb{E}\Big\{ \boldsymbol{s}_n \boldsymbol{s}_n^H | \mathcal{H}_1, \widehat{\mathcal{H}}_{0,n} \Big\} = \Big(\widehat{\gamma}_n^1 P_{\mathrm{t}} + \sigma_{v_n}^2 + \sigma_p^2 \Big) \boldsymbol{I}. \tag{18b}$$

After substituting (17) into (16), $\widehat{h}_n$ reduces to

$$\widehat{h}_n = \frac{\gamma_n \sqrt{P_{\mathrm{t}}}}{\gamma_n P_{\mathrm{t}} N_{\mathrm{t}} + \sigma_{v_n}^2 + \omega_{1,n} \sigma_p^2} \sum_{m=1}^{N_{\mathrm{t}}} s_n[m], \tag{19}$$

where $\sigma_p^2 = P_p \delta_q$. The estimation error is $\widetilde{h}_n = h_n - \widehat{h}_n$, where $\widehat{h}_n$ and $\widetilde{h}_n$ are orthogonal random variables [45], and $\widehat{h}_n$ and $\widetilde{h}_n$ are zero mean. Approximating $q[m]p[m]$ as a zero-mean Gaussian random variable with variance σ_p^2, we find that the estimate $\widehat{h}_n$ given $\widehat{\mathcal{H}}_{0,n}$ is distributed as a Gaussian mixture random variable [6]. Let $\widehat{\gamma}_n$ and $\widetilde{\gamma}_n$, represent the variances of $\widehat{h}_n$ and $\widetilde{h}_n$, respectively. Also, Let $\widehat{\gamma}_n^0$ and $\widehat{\gamma}_n^1$ represent the variances of $\widehat{h}_n$ under $\{\mathcal{H}_0, \widehat{\mathcal{H}}_{0,n}\}$ and $\{\mathcal{H}_1, \widehat{\mathcal{H}}_{0,n}\}$, respectively. We have

$$\widehat{\gamma}_n^0 = \mathbb{VAR}\Big\{ \widehat{h}_n | \mathcal{H}_0, \widehat{\mathcal{H}}_{0,n} \Big\} = \frac{\gamma_n^2 P_{\mathrm{t}} N_{\mathrm{t}} \big(\gamma_n P_{\mathrm{t}} N_{\mathrm{t}} + \sigma_{v_n}^2 \big)}{\big(\gamma_n P_{\mathrm{t}} N_{\mathrm{t}} + \sigma_{v_n}^2 + \omega_{1,n} \sigma_p^2 \big)^2}, \tag{20a}$$

$$\widehat{\gamma}_n^1 = \mathbb{VAR}\Big\{ \widehat{h}_n | \mathcal{H}_1, \widehat{\mathcal{H}}_{0,n} \Big\} = \frac{\gamma_n^2 P_{\mathrm{t}} N_{\mathrm{t}} \big(\gamma_n P_{\mathrm{t}} N_{\mathrm{t}} + \sigma_{v_n}^2 + \sigma_p^2 \big)}{\big(\gamma_n P_{\mathrm{t}} N_{\mathrm{t}} + \sigma_{v_n}^2 + \omega_{1,n} \sigma_p^2 \big)^2}. \tag{20b}$$

Therefore, $\widehat{\gamma}_n = \omega_{0,n} \widehat{\gamma}_n^0 + \omega_{1,n} \widehat{\gamma}_n^1$. Also, let $\widetilde{\gamma}_n^0$ and $\widetilde{\gamma}_n^1$ indicate the variances of $\widetilde{h}_n$ under $\{\mathcal{H}_0, \widehat{\mathcal{H}}_{0,n}\}$ and $\{\mathcal{H}_1, \widehat{\mathcal{H}}_{0,n}\}$, respectively. We have

$$\widetilde{\gamma}_n^0 = \mathbb{VAR}\Big\{ \widetilde{h}_n | \mathcal{H}_0, \widehat{\mathcal{H}}_{0,n} \Big\} = \gamma_n - \widehat{\gamma}_n^0, \tag{21a}$$

$$\widetilde{\gamma}_n^1 = \mathbb{VAR}\Big\{ \widetilde{h}_n | \mathcal{H}_1, \widehat{\mathcal{H}}_{0,n} \Big\} = \gamma_n - \widehat{\gamma}_n^1. \tag{21b}$$

Hence, $\widetilde{\gamma}_n = \omega_{0,n} \widetilde{\gamma}_n^0 + \omega_{1,n} \widetilde{\gamma}_n^1$. For ideal spectrum sensing, we get $\omega_{0,n} = 1$ and $\omega_{1,n} = 0$ and $\widehat{h}_n$ becomes Gaussian. Let $F_{\widehat{g}_n}^{\varepsilon}(x)$ denote the CDF of $\widehat{g}_n$ under $\{\mathcal{H}_\varepsilon, \widehat{\mathcal{H}}_{0,n}\}$ for $\varepsilon = 0, 1$. Note that under $\{\mathcal{H}_\varepsilon, \widehat{\mathcal{H}}_{0,n}\}$ for $\varepsilon = 0, 1$, $\widehat{h}_n$ is zero mean complex Gaussian. Hence, under $\{\mathcal{H}_\varepsilon, \widehat{\mathcal{H}}_{0,n}\}$ for $\varepsilon = 0, 1$, $\widehat{g}_n$ is an exponential random variable with mean $\widehat{\gamma}_n^{\varepsilon}$ and CDF

$$F_{\widehat{g}_n}^{\varepsilon}(x) = 1 - e^{\frac{-x}{\widehat{\gamma}_n^{\varepsilon}}}. \tag{22}$$

The CDF of $\widehat{g}_n$, denoted as $F_{\widehat{g}_n}^{\varepsilon}(x)$, can be expressed in terms of $F_{\widehat{g}_n}^{0}(x)$ and $F_{\widehat{g}_n}^{1}(x)$ as the following:

$$F_{\widehat{g}_n}(x) = \omega_{0,n} F_{\widehat{g}_n}^{0}(x) + \omega_{1,n} F_{\widehat{g}_n}^{1}(x). \tag{23}$$

After channel estimation, the AP feeds back the channel gains $\widehat{g}_n = |\widehat{h}_n|^2$ over a feedback link to SU$_n$.

V. Data Transmission Phase

After channel probing phase, SU$_n$ enters this phase. We note that entering this phase is only possible, if in spectrum sensing phase the outcome of the binary detector is $\widehat{\mathcal{H}}_{0,n}$. During this phase, SU$_n$ sends Gaussian data symbols to the AP, while it adapts its transmission power according to information provided by the AP through the feedback channel about SU$_n$–AP link as well as its battery state. In particular, SU$_n$ transmits N_{d} zero-mean i.i.d. complex Gaussian symbols $x_n[m]$ for $m = 1, \ldots, N_{\mathrm{d}}$ with power $P_{k,n} = \alpha_{k,n} p_{\mathrm{u}}$, when the battery is at state k and $\alpha_{k,n}$ is given in (2). Let $s_n[m]$ denote the discrete-time representation of received signal at the AP from SU$_n$. Due to error in spectrum sensing, we need to distinguish the signal model for $s_n[m]$ under $\mathcal{H}_0$ and $\mathcal{H}_1$. We have

$$\begin{aligned} &\mathcal{H}_0, \widehat{\mathcal{H}}_{0,n} : s_n[m] = h_n x_n[m] + v_n[m], \\ &\mathcal{H}_1, \widehat{\mathcal{H}}_{0,n} : s_n[m] = h_n x_n[m] + q[m]p[m] + v_n[m]. \end{aligned} \tag{24}$$

Substituting $h_n = \widehat{h}_n + \widetilde{h}_n$ in (24), we reach at[6]

$$\begin{aligned} \mathcal{H}_0, \widehat{\mathcal{H}}_{0,n} &: s_n[m] = \widehat{h}_n x_n[m] + \overbrace{\widetilde{h}_n x_n[m] + v_n[m]}^{\text{new noise } \eta_{n,0}[m]}, \\ \mathcal{H}_1, \widehat{\mathcal{H}}_{0,n} &: s_n[m] = \widehat{h}_n x_n[m] \\ &\qquad + \underbrace{\widetilde{h}_n x_n[m] + q[m]p[m] + v_n[m]}_{\text{new noise } \eta_{n,1}[m]}, \end{aligned} \tag{25}$$

where the new noise terms depend on $\widetilde{h}_n$. Given $\widehat{g}_n$ at the AP, we obtain an achievable rate expression for a time slot by considering symbol-wise mutual information between channel input and output over the duration of N_{d} data symbols as follows

$$R_n = \frac{W D_{\mathrm{d}}}{N_{\mathrm{d}}} \times \sum_{m=1}^{N_{\mathrm{d}}} \Big[\beta_{0,n} \mathbb{E}\Big\{ I\Big(x_n[m]; s_n[m] | \widehat{g}_n, \mathcal{H}_0, \widehat{\mathcal{H}}_{0,n} \Big) \Big\} + \beta_{1,n} \mathbb{E}\Big\{ I\Big(x_n[m]; s_n[m] | \widehat{g}_n, \mathcal{H}_1, \widehat{\mathcal{H}}_{0,n} \Big) \Big\} \Big], \tag{26}$$

[6]We note that under $\mathcal{H}_\varepsilon$, our channel model $h_n = \widehat{h}_n + \widetilde{h}_n$ can be extended to include both the effects of channel estimation error and delayed feedback due to SU$_n$'s mobility. In particular, we can model $h_n = \chi \overline{h}_n + z_n$, where the parameter $\chi = J_0(2\pi v T_{\mathrm{f}}/\lambda)$ is from Jakes' model for Rayleigh fading [46], v is the velocity of SU$_n$, and λ is the wavelength of transmit signal, $\overline{h}_n$ is the outdated CSI available at SU$_n$, and $z_n \sim \mathcal{CN}(0, (1 - \chi^2)\widehat{\gamma}_n^{\varepsilon} + \widetilde{\gamma}_n^{\varepsilon})$. Substituting this channel model in (24) we reach at a signal model that is different from (25), which can be used to derive a new rate lower bound $R_{n,\mathrm{LB}}$.

where $D_{\rm d} = \tau_{\rm d}/T_{\rm f}$ is the fraction of the time slot used for data transmission and the expectations in (26) are taken over the conditional probability density functions (pdfs) of $\widehat{g}_n$ given $\{\mathcal{H}_\varepsilon, \widehat{\mathcal{H}}_{0,n}\}$ for $\varepsilon = 0, 1$. To characterize R_n in (26) we need to find $\mathbb{E}\{I(x_n[m]; s_n[m]|\widehat{g}_n, \mathcal{H}_\varepsilon, \widehat{\mathcal{H}}_{0,n})\}$. Exploiting the chain rule we can rewrite this expectation as follows

$$\mathbb{E}\Big\{ I\Big(x_n[m]; s_n[m]\big|\widehat{g}_n, \mathcal{H}_\varepsilon, \widehat{\mathcal{H}}_{0,n}\Big)\Big\} = \sum_{k=0}^{K} \zeta_{k,n}\, I\Big(x_n[m]; s_n[m]\big|\widehat{g}_n, k, \mathcal{H}_\varepsilon, \widehat{\mathcal{H}}_{0,n}\Big). \quad (27)$$

Note that $I(x_n[m]; s_n[m]|\widehat{g}_n, \mathcal{H}_\varepsilon, \widehat{\mathcal{H}}_{0,n})$ in (27) is the mutual information between $x_n[m]$ and $s_n[m]$ when the battery state is k, given $\widehat{g}_n$ and $\{\mathcal{H}_\varepsilon, \widehat{\mathcal{H}}_{0,n}\}$. From now on, we drop the variable m in $x_n[m]$ and $s_n[m]$ for brevity of the presentation. Focusing on $I(x_n; s_n|\widehat{g}_n, \mathcal{H}_\varepsilon, \widehat{\mathcal{H}}_{0,n})$, we have

$$I\Big(x_n; s_n\big|\widehat{g}_n, k, \mathcal{H}_\varepsilon, \widehat{\mathcal{H}}_{0,n}\Big) = h\Big(x_n\big|\widehat{g}_n, k, \widehat{\mathcal{H}}_{0,n}, \mathcal{H}_\varepsilon\Big) - h\Big(x_n\big|s_n, \widehat{g}_n, k, \widehat{\mathcal{H}}_{0,n}, \mathcal{H}_\varepsilon\Big), \quad (28)$$

where $h(\cdot)$ is the differential entropy. Consider the first term in (28). Since $x_n \sim \mathcal{CN}(0, P_{k,n})$ we have $h(x_n|\widehat{g}_n, k, \widehat{\mathcal{H}}_{0,n}, \mathcal{H}_\varepsilon) = \log_2(\pi e P_{k,n})$. Consider the second term in (28). Due to channel estimation error, the new noises $\eta_{n,\varepsilon}$'s in (25) are non-Gaussian and this term does not have a closed form expression. Hence, similar to [34], [38], [47] we employ bounding techniques to find an upper bound on this term. This term is upper bounded by the entropy of a Gaussian random variable with the variance $\Theta_{\rm M}^{n,\varepsilon}$

$$\Theta_{\rm M}^{n,\varepsilon} = \mathbb{E}\Big\{\big|x_n - \mathbb{E}\Big\{x_n|\widehat{g}_n, k, \widehat{\mathcal{H}}_{0,n}, \mathcal{H}_\varepsilon\Big\}\big|^2\Big\}, \quad (29)$$

where the expectations are taken over the conditional pdf of x_n given $s_n, \widehat{g}_n, k, \widehat{\mathcal{H}}_{0,n}, \mathcal{H}_\varepsilon$. In fact, $\Theta_{\rm M}^{i,\varepsilon}$ is the mean square error (MSE) of the MMSE estimate of x_n given $s_n, \widehat{g}_n, k, \widehat{\mathcal{H}}_{0,n}, \mathcal{H}_\varepsilon$. Using minimum variance property of MMSE estimator, we have $\Theta_{\rm M}^{n,\varepsilon} \leq \Theta_{\rm L}^{n,\varepsilon}$, where $\Theta_{\rm L}^{n,\varepsilon}$ is the MSE of the LMMSE estimate of x_n given $s_n, \widehat{g}_n, k, \widehat{\mathcal{H}}_{0,n}, \mathcal{H}_\varepsilon$. Combining all, we find $h(x_n|s_n, \widehat{g}_n, k, \widehat{\mathcal{H}}_{0,n}, \mathcal{H}_\varepsilon) \leq \log_2(\pi e \Theta_{\rm L}^{n,\varepsilon})$ and $I(x_n; s_n|\widehat{g}_n, k, \widehat{\mathcal{H}}_{0,n}, \mathcal{H}_\varepsilon) \geq \log_2(P_{k,n}/\Theta_{\rm L}^{n,\varepsilon})$ where

$$\Theta_{\rm L}^{n,\varepsilon} = \frac{P_{k,n}\sigma^2_{\eta_{n,\varepsilon}}}{\sigma^2_{\eta_{n,\varepsilon}} + \widehat{g}_n P_{k,n}}, \quad (30)$$

$$\sigma^2_{\eta_{n,\varepsilon}} = \widetilde{\gamma}_n^{\varepsilon} P_{k,n} + \sigma^2_{v_n} + \varepsilon\sigma_p^2. \quad (31)$$

At the end, we obtain the lower bounds as follow

$$I\Big(x_n; s_n\big|\widehat{g}_n, k, \widehat{\mathcal{H}}_{0,n}, \mathcal{H}_0\Big) \geq \log_2\Big(1 + \widehat{g}_n b_{k,n}^0\Big), \quad (32a)$$

$$I\Big(x_n; s_n\big|\widehat{g}_n, k, \widehat{\mathcal{H}}_{0,n}, \mathcal{H}_1\Big) \geq \log_2\Big(1 + \widehat{g}_n b_{k,n}^1\Big), \quad (32b)$$

where

$$b_{k,n}^0 = \frac{P_{k,n}}{\big(\widetilde{\gamma}_n^0 P_{k,n} + \sigma^2_{v_n}\big)}, \quad b_{k,n}^1 = \frac{P_{k,n}}{\big(\widetilde{\gamma}_n^1 P_{k,n} + \sigma^2_{v_n} + \sigma_p^2\big)}. \quad (33)$$

Substituting equations (27) and (32) in (26) and noting that the symbol-wise mutual information between channel input and output for $N_{\rm d}$ data symbols are equal we reach at

$$\begin{aligned} R_n &\geq R_{n,\rm LB} \\ &= D_{\rm d}\beta_{0,n} W \sum_{k=0}^{K} \zeta_{k,n} \mathbb{E}\Big\{\log_2\Big(1 + \widehat{g}_n b_{k,n}^0\Big)|\mathcal{H}_0\Big\} \\ &\quad + D_{\rm d}\beta_{1,n} W \sum_{k=0}^{K} \zeta_{k,n} \mathbb{E}\Big\{\log_2\Big(1 + \widehat{g}_n b_{k,n}^1\Big)|\mathcal{H}_1\Big\}. \end{aligned} \quad (34)$$

Next, we compute the conditional expectations in (34), in which we take average over $\widehat{g}_n$, given $\mathcal{H}_\varepsilon$. Using (3) and (4c) we have

$$\begin{aligned} &\mathbb{E}\Big\{\log_2\Big(1 + \widehat{g}_n b_{k,n}^{\varepsilon}\Big)|\mathcal{H}_\varepsilon\Big\} \\ &= \sum_{i=1}^{\lfloor k\Omega_n\rfloor - \alpha_{\rm t}} \int_{a_{i,k,n}}^{c_{i,k,n}} \log_2\Big(1 + {\rm S}_{i,n}^{\varepsilon}\, x\Big) f_{\widehat{g}_n}^{\varepsilon}(x)\, dx \\ &= \sum_{i=1}^{\lfloor k\Omega_n\rfloor - \alpha_{\rm t}} V_k({\rm S}_{i,n}^{\varepsilon}, \widehat{\gamma}_n^{\varepsilon}) \end{aligned} \quad (35a)$$

in which

$$\begin{aligned} {\rm S}_{i,n}^0 &= \frac{ip_{\rm u}}{\big(\widetilde{\gamma}_n^0 ip_{\rm u} + \sigma^2_{v_n}\big)}, \\ {\rm S}_{i,n}^1 &= \frac{ip_{\rm u}}{\big(\widetilde{\gamma}_n^1 ip_{\rm u} + \sigma^2_{v_n} + \sigma_p^2\big)}, \end{aligned} \quad (35b)$$

$$\begin{aligned} V_k\big({\rm S}_{i,n}, \widehat{\gamma}_n\big) &= M\big(c_{i,k,n}, {\rm S}_{i,n}, \widehat{\gamma}_n\big) \\ &\quad - M\big(a_{i,k,n}, {\rm S}_{i,n}, \widehat{\gamma}_n\big), \end{aligned} \quad (35c)$$

and

$$\begin{aligned} M(x, {\rm S}, w) &= \int \log_2(1 + {\rm S}\, x) \frac{e^{\frac{-x}{w}}}{w} dx \\ &= \frac{e^{\frac{1}{{\rm S}\, w}}}{\ln(2)}\ {\rm Ei}\bigg(\frac{-x}{w} - \frac{1}{{\rm S}\, w}\bigg) - e^{\frac{-x}{w}} \log_2(1 + {\rm S}\, x). \end{aligned} \quad (36)$$

Also, $c_{i,k,n}$ and $a_{i,k,n}$ are given in (4c). Substituting (35a) in (34) we reach to

$$\begin{aligned} R_{n,\rm LB} &= D_{\rm d}\beta_{0,n} W \sum_{k=\alpha_{\rm t}+1}^{K} \sum_{i=1}^{\lfloor k\Omega_n\rfloor - \alpha_{\rm t}} \zeta_{k,n} V_k\Big({\rm S}_{i,n}^0, \widehat{\gamma}_n^0\Big) \\ &\quad + D_{\rm d}\beta_{1,n} W \sum_{k=\alpha_{\rm t}+1}^{K} \sum_{i=1}^{\lfloor k\Omega_n\rfloor - \alpha_{\rm t}} \zeta_{k,n} V_k\Big({\rm S}_{i,n}^1, \widehat{\gamma}_n^1\Big). \end{aligned} \quad (37)$$

We note that the lower bounds in (32) are achieved when the new noises $\eta_{n,0}, \eta_{n,1}$ in (25) are regarded as worst-case Gaussian noise and hence the MMSE and LMMSE of x_n given $s_n, \widehat{g}_n, k, \widehat{\mathcal{H}}_{0,n}, \mathcal{H}_\varepsilon$ coincide. Given the rate lower bound $R_{n,\rm LB}$ for SU$_n$, the uplink sum-rate lower bound for all SU$_n$'s is

$$R_{\rm LB} = \sum_{n=1}^{N_{\rm u}} R_{n,\rm LB}. \quad (38)$$

So far, we have established a lower bound on the achievable sum-rate. Next, we characterize the average inference constraint (AIC). Suppose $\overline{I}_{\rm av}$ is the maximum allowed average interference power, i.e., the average interference power that collective SUs impose on $\mathrm{PU_{rx}}$ cannot exceed $\overline{I}_{\rm av}$. To satisfy AIC, we have

$$\sum_{n=1}^{N_{\rm u}} I_n \leq \overline{I}_{\rm av}, \tag{39}$$

where I_n is the average interference power that SU_n imposes on $\mathrm{PU_{rx}}$. We find

$$I_n = \beta_{1,n}\mathbb{E}\{z_n\}[D_{\rm d}\mathbb{E}\{P_n(\widehat{g}_n)\} + D_{\rm t}P_{\rm t}] \tag{40}$$

where $D_{\rm t} = \tau_{\rm t}/T_{\rm f}$ and the expectation is over the conditional pdfs of $\widehat{g}_n$ under $\{\mathcal{H}_1, \widehat{\mathcal{H}}_{0,n}\}$. Considering the right side of (40), we note that the first term is the average interference power imposed on $\mathrm{PU_{rx}}$ when SU_n transmits data symbols, and the second term is the average interference imposed on $\mathrm{PU_{rx}}$ when SU_n sends training symbols for channel estimation at the AP. Using (3) we compute the term with expectation inside (40) as follows

$$\begin{aligned}\mathbb{E}\{P_n(\widehat{g}_n)\} &= \sum_{k=0}^{K}\zeta_{k,n}\sum_{i=0}^{K}\Pr\big(\alpha_{k,n}=i|\mathcal{H}_1\big)\,ip_{\rm u}\\ &= \sum_{k=\alpha_{\rm t}+1}^{K}\zeta_{k,n}\sum_{i=1}^{\lfloor k\Omega_n\rfloor-\alpha_{\rm t}}\psi^1_{i,k,n}\,ip_{\rm u}.\end{aligned} \tag{41}$$

Substituting (41) into (39), we can rewrite the AIC in (39) as

$$\begin{aligned}&\sum_{n=1}^{N_{\rm u}}\beta_{1,n}\delta_{z_n}\left[\sum_{k=\alpha_{\rm t}+1}^{K}\zeta_{k,n}\sum_{i=1}^{\lfloor k\Omega_n\rfloor-\alpha_{\rm t}}\psi^1_{i,k,n}\,ip_{\rm u} + D_{\rm t}P_{\rm t}\right]\\ &\quad\leq \overline{I}_{\rm av}.\end{aligned} \tag{42}$$

For ideal spectrum sensing we get $\beta_{1,n}=0$ in (14), implying that data transmission from SUs to the AP does not cause interference on $\mathrm{PU_{rx}}$ and the left-hand side of (42) becomes zero, i.e., the AIC is always satisfied.

Next, we examine how spectrum sensing error and channel estimation error affect $R_{\rm LB}$ and AIC expressions. First, spectrum sensing error affects AIC via $\beta_{1,n}$, and $R_{\rm LB}$ via $\beta_{0,n}$ and $\beta_{1,n}$. Recall $\beta_{0,n}, \beta_{1,n}$ depend on $\pi_0, P_{\mathrm{fa}_n}, P_{\mathrm{d}_n}$ (see (14)). Second, channel estimation error affects AIC via $D_{\rm t}, \psi^1_{i,k,n}$, and $R_{\rm LB}$ via $\widetilde{\gamma}^{\varepsilon}_n$.

Having the mathematical expressions for $R_{\rm LB}$ and AIC, our goal is to optimize the set of transmission parameters $\{\Omega_n, \theta_n\}$ for all SUs such that $R_{\rm LB}$ is maximized, subject to the AIC. To inspect the underlying trade-offs between decreasing the average interference power imposed by SU_n's on $\mathrm{PU_{rx}}$ and increasing the uplink sum-rate lower bound $R_{\rm LB}$, we note that increasing data symbol transmission power $P_{k,n}$ increases $R_{\rm LB}$. However, it increases the average interference power. Aiming to strike a balance between increasing $R_{\rm LB}$ and decreasing the imposed average interference power, we seek the optimal $\{\Omega_n, \theta_n\}_{n=1}^{N_{\rm u}}$ such that $R_{\rm LB}$ in (34) is maximized, subject to AIC given in (42). In other words, we are interested in solving the following constrained optimization problem

$$\begin{aligned}(\mathrm{P1})\quad \underset{\{\Omega_n,\,\theta_n\}_{n=1}^{N_{\rm u}}}{\text{Maximize}}\quad & R_{\rm LB}\\ \text{s.t.:}\quad & \Omega_n \in [0,1],\ \forall n\\ & \theta_n \geq 0,\ \forall n\\ & \boldsymbol{\zeta}_n = (\boldsymbol{\Phi}_n - \boldsymbol{I} + \boldsymbol{B})^{-1}\mathbf{1},\ \forall n\\ & \text{AIC in (43) issatisfied.}\end{aligned}$$

Problem (P1) is not convex with respect to $\{\Omega_n, \theta_n\}_{n=1}^{N_{\rm u}}$. Unfortunately, the objective function and the constraints in (P1) are *not differentiable* with respect to $\{\Omega_n, \theta_n\}_{n=1}^{N_{\rm u}}$. Hence, existing gradient-based algorithms for solving non-convex optimization problems cannot be used to solve (P1). We resort to a grid-based search method, which requires $2N_{\rm u}$-dimensional search over the search space $[0,1]^{N_{\rm u}} \times [0,\infty)^{N_{\rm u}}$.

To reduce the computation complexity of solving (P1), we propose to decompose (P1) to $N_{\rm u}$ sub-problems corresponding to $N_{\rm u}$ SUs. To achieve such decomposition, we assume that I_n in (40) cannot exceed $\overline{I}_{\rm av}/N_{\rm u}$. Let $(\mathrm{SP1\text{-}SU}_n)$ refer to the sub-problem corresponding to SU_n. We have

$$\begin{aligned}(\mathrm{SP1\text{-}SU}_n)\quad \underset{\{\Omega_n,\,\theta_n\}}{\text{Maximize}}\quad & R_{n,\rm LB}\\ \text{s.t.:}\quad & \Omega_n \in [0,1],\\ & \theta_n \geq 0,\\ & \boldsymbol{\zeta}_n = (\boldsymbol{\Phi}_n - \boldsymbol{I} + \boldsymbol{B})^{-1}\,\mathbf{1},\\ & I_n \leq \overline{I}_{\rm av}/N_{\rm u}.\end{aligned}$$

We solve sub-problem $(\mathrm{SP1\text{-}SU}_n)$ for $n = 1, \ldots, N_{\rm u}$, using a grid-based search method, which requires 2-dimensional search over the search space $[0,1]\times[0,\infty)$. To curb the computational complexity of these searches, we can limit θ_n's to a maximum value, denoted as $\theta_{\max}$. We refer to the solutions obtained from solving (P1) and solving $N_{\rm u}$ sub-problems, respectively, the "optimal" and the "sub-optimal" solutions. Clearly, the accuracy of these solutions depend on the resolution of the grid-based searches. We call the former solution the "optimal", in the sense that it is the best achievable solution, and the latter solution the "sub-optimal", in the sense that solving $N_{\rm u}$ sub-problems always yield a sub-optimal solution, with respect to solving (P1), since AIC in (P1) is coupled across all SUs. When $\overline{I}_{\rm av}$ in (39) is large enough such that AIC is not active, the "optimal" and "sub-optimal" solutions become identical. In the following, we compare the computational complexity of finding the "optimal" and "sub-optimal" solutions.

For finding both the "optimal" and the "sub-optimal" solutions, SU_n needs to perform two tasks for each point in its grid-based search: task (i) forming $\boldsymbol{\Phi}_n$ and solving (10) to find $\boldsymbol{\zeta}_n$, task (ii) calculating $R_{n,\rm LB}$ and I_n. Our numerical results show that for a fixed Ω_n, θ_n, the computational complexity of task (i) and task (ii) are $\mathcal{O}(K^{3.1})$ and $\mathcal{O}(K^{2.1})$, respectively. Assuming that the intervals $[0,1]$ and $[0,\theta_{\max}]$ are divided into N_Ω and N_θ sub-intervals, respectively, we realize that SU_n needs to perform task (i) and task (ii) for $N_\Omega N_\theta$ times in total. Therefore, the computational complexity of finding the "sub-optimal" solution is $\mathcal{O}(N_{\rm u}N_\Omega N_\theta(K^{3.1}+K^{2.1}))$, which can be simplified to $\mathcal{O}(N_{\rm u}N_\Omega N_\theta K^{3.1})$.

TABLE II
SIMULATION PARAMETERS

Parameter	Value	Parameter	Value
P_p	1 watts	$\sigma_{v_n}^2$	1
π_0	0.7	$\sigma_{w_n}^2$	1
$\tau_{\rm t}$	0.1 ms	$\alpha_{\rm t}$	1
$\tau_{\rm s}$	1 ms	$\overline{P}_{\rm d}$	0.85
$T_{\rm f}$	10 ms	W	10 KHz
$e_{\rm u}$	0.01	δ_q	1

To solve (P1), however, the leftmost summation in (42) must be computed for all combinations of $\{\Omega_n, \theta_n\}_{n=1}^{N_{\rm u}}$ and its computational complexity is $\mathcal{O}((N_\Omega N_\theta K^{2.1})^{N_{\rm u}})$. Therefore, the computational complexity of finding the "optimal" solution is $\mathcal{O}((N_\Omega N_\theta K^{2.1})^{N_{\rm u}} + N_{\rm u} N_\Omega N_\theta K^{3.1})$, which for $N_{\rm u} \geq 2$ can be simplified to $\mathcal{O}((N_\Omega N_\theta K^{2.1})^{N_{\rm u}})$. We note that the computational complexity of obtaining the "optimal" and the "sub-optimal" solutions grow exponentially and linearly, respectively, in $N_{\rm u}$.

VI. SIMULATION RESULTS

In this section we corroborate our analysis on constrained maximization of the achievable uplink sum-rate lower bound with MATLAB simulations, and examine how the optimized uplink sum-rate lower bound depends on the average number of harvesting energy packets ρ_n, the maximum allowed average interference power $\overline{I}_{\rm av}$, the duration of spectrum sensing phase $\tau_{\rm s}$, the number of consumed cells of energy for channel probing $\alpha_{\rm t}$, and the size of the battery K. Our simulation parameters are given in Table II.

• *Spectrum Sensing- Channel Probing-Data Transmission Trade-offs:* To explore these trade-offs, in this section we let $N_{\rm u} = 1$ and examine how the rate lower bound $R_{\rm LB}$ in (38) for a single user changes when we vary $\tau_{\rm s}$, or $\alpha_{\rm t}$. The simulation parameters, except for $\alpha_{\rm t}, \tau_{\rm s}, \sigma_w^2, \sigma_v^2$ are given in Table II.[7]

Fig. 6(a) shows $R_{\rm LB}$ versus $\tau_{\rm s}$ for two values of the energy harvesting parameter $\rho = 15, 16, \sigma_w^2 = \sigma_v^2 = 1$ and $\alpha_{\rm t} = 1$. This figure suggests that there exists a trade-off between $\tau_{\rm s}$ and $R_{\rm LB}$. On the positive side, as $\tau_{\rm s}$ (or equivalently $N_{\rm s}$) increases, the accuracy of the energy detector for spectrum sensing increases (i.e., $P_{{\rm fa}_n}$ in (12b) decreases). A more accurate spectrum sensing can reveal new opportunities for SU$_n$ to be exploited for its data transmission, that can increase $R_{\rm LB}$. On the negative side, as $\tau_{\rm s}$ increases, the duration of data transmission phase $\tau_{\rm d} = T_{\rm f} - \tau_{\rm s} - \tau_{\rm t}$ decreases. This trade-off between spectrum sensing and data transmission indicates that, given the parameters (including $\alpha_{\rm t}$), there is an optimal $\tau_{\rm s}$, denoted as $\tau_{\rm s}^*$ in Fig. 6(a), that maximizes $R_{\rm LB}$. For instance, for $\rho = 15, 16$ we have $\tau_{\rm s}^* = 0.6$, 0.75 ms.

Fig. 6(b) plots $R_{\rm LB}$ versus $\alpha_{\rm t}$ for $\rho = 18, 20$, $\tau_{\rm s} = 1$ ms and $\sigma_w^2 = \sigma_v^2 = 5$. This figure suggests that a trade-off exists between $\alpha_{\rm t}$ and $R_{\rm LB}$. On the positive side, as $\alpha_{\rm t}$ increases, the accuracy of channel probing (measured by the variance of channel estimation error in (20)) improves. A more accurate channel probing can increase $R_{\rm LB}$. On the negative side, as $\alpha_{\rm t}$ increases, the available energy for data transmission decreases. This trade-off between channel probing and data transmission shows that, given the parameters (including $\tau_{\rm s}$), there is an optimal $\alpha_{\rm t}$, denoted as $\alpha_{\rm t}^*$ in Fig. 6(b), that maximizes $R_{\rm LB}$. For instance, for $\rho = 15, 16$ we have $\alpha_{\rm t}^* = 4$. The x-axis in Fig. 6(b) can be converted to the normalized channel estimation error variance $\widetilde{\gamma}/\gamma$.

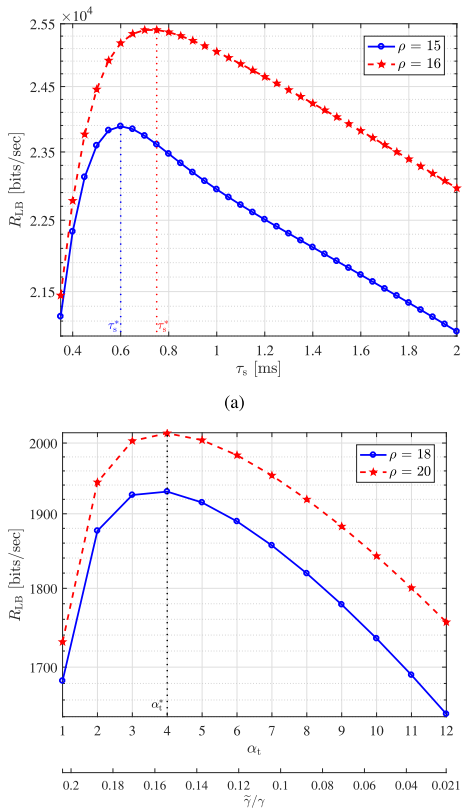

Fig. 6. (a) $R_{\rm LB}$ versus $\tau_{\rm s}$ for $K = 80$, $\theta = 0.25, \Omega = 0.35, \sigma_w^2 = \sigma_v^2 = 1$, (b) $R_{\rm LB}$ versus $\alpha_{\rm t}$ for $K = 200$, $\theta = 0.25, \Omega = 0.35, \sigma_w^2 = \sigma_v^2 = 5$.

• *Effect of the Optimization Variables $\boldsymbol{\Omega}, \boldsymbol{\theta}$:* In this section, we let $N_{\rm u} = 1$ and we illustrate how the entries of the steady-state probability vector $\boldsymbol{\zeta}$ in (10), $R_{\rm LB}$ in (38) for a single user, and the battery outage probability $P_b^{\rm Out}$ defined below, the spectral efficiency $\eta_{\rm SE}$ and the energy efficiency $\eta_{\rm EE}$ defined below, depend on the optimization variables Ω and θ. We define $P_{b_n}^{\rm Out}$ as the steady-state probability of the battery of SU$_n$ being equal or lower than $\alpha_{\rm t}$. When the battery is at outage, it cannot yield energy for data transmission or channel probing. We have

$$P_{b_n}^{\rm Out} = \Pr(\mathcal{B}_n \leq \alpha_{\rm t}) = \sum_{k=0}^{\alpha_{\rm t}} \zeta_{k,n}. \tag{43}$$

We define the spectral efficiency of our CR system, denoted as $\eta_{\rm SE}$ and measured in bits/sec/Hz, as

$$\eta_{\rm SE} = \frac{R_{\rm LB}}{\text{total available bandwidth}} = \frac{R_{\rm LB}}{MW} \tag{44}$$

[7]Note that the variances of channel estimate and corresponding estimation error in (20) depend on the product $P_{\rm t} N_{\rm t} = \alpha_{\rm t} e_{\rm u} f_{\rm s}$ and is independent of $\tau_{\rm t}$. That is the reason, instead of $\tau_{\rm t}$, we consider varying $\alpha_{\rm t}$, to understand channel probing trade-offs.

Inspired by [48], we define the energy efficiency of our CR system, denoted as $\eta_{\rm EE}$ and measured in bits/Hz/Joule, as

$$\eta_{\rm EE} = \frac{\eta_{\rm SE}}{\text{average transmit power of all SUs}} \tag{45}$$

Let $\overline{P}$ denote the average transmit power of all SUs during channel probing and data transmission phases in our CR system. We find $\overline{P}$ as the following

$$\begin{aligned}\overline{P} = D_{\rm d} \sum_{n=1}^{N_{\rm u}} \sum_{k=\alpha_{\rm t}+1}^{K} \zeta_{k,n} \\ \times \sum_{i=1}^{\lfloor k\Omega_n \rfloor - \alpha_{\rm t}} ip_{\rm u}\left[\beta_{0,n}\psi^0_{i,k,n} + \beta_{1,n}\psi^1_{i,k,n}\right] \\ + D_{\rm t}P_{\rm t}\sum_{n=1}^{N_{\rm u}} \widehat{\pi}_{0,n}.\end{aligned} \tag{46}$$

The simulation parameters are given in Table II. Also, we let $\boldsymbol{\gamma} = 2, \boldsymbol{\delta}_u = 1, \boldsymbol{\delta}_z = 1$. Fig. 7(a) illustrates $R_{\rm LB}$ for a single user versus Ω for $\rho = 15, 20$. We observe that $R_{\rm LB}$ is neither a convex nor a concave function of Ω. This figure suggests that there is an optimal Ω, which we denote as Ω^*, that maximizes $R_{\rm LB}$. Starting from small values of Ω, as Ω increases (until it reaches the value Ω^*), $R_{\rm LB}$ increases, because the harvested energy can recharge the battery and can yield more power for data transmission. However, when Ω exceeds Ω^*, the harvested and stored energy cannot support the data transmission and $R_{\rm LB}$ decreases. Moreover, as ρ increases, $R_{\rm LB}$ increases as well. The behavior of $R_{\rm LB}$ versus θ is shown in Fig. 7(b) for $\rho = 15, 18$. We observe that $R_{\rm LB}$ is neither a convex nor a concave function of θ. Similar to Ω, there is an optimal θ, which we denote as θ^*, that maximizes $R_{\rm LB}$. Starting from small values of θ, as θ increases (until it reaches θ^*), $R_{\rm LB}$ increases. However, when θ exceeds θ^*, $R_{\rm LB}$ decreases.

Fig. 8 plots the entries of the steady-state probability vector $\boldsymbol{\zeta}$ versus k for $\Omega = 0.45, 0.3$ and $\theta = 0.2$. Fig. 9 plots the entries of $\boldsymbol{\zeta}$ versus k for $\theta = 0.1, 0.5$ and $\Omega = 0.35$. To quantify the effect of Ω and θ on the entries of $\boldsymbol{\zeta}$ we define the average energy stored at the battery of SU_n as

$$\overline{\mathcal{B}}_n = \mathbb{E}\{\mathcal{B}_n\} = \sum_{k=0}^{K} k\,\zeta_{k,n}, \tag{47}$$

where the largest possible value for $\overline{\mathcal{B}}_n$ is K. Considering Figs. 8(a) and 8(b), we find $\overline{\mathcal{B}}^{(a)} = 16.97$ for $\Omega = 0.45$, implying that the battery is near empty, and $\overline{\mathcal{B}}^{(b)} = 66.30$ for $\Omega = 0.30$, implying that the battery is near full. Considering Figs. 9(a) and 9(b), we find $\overline{\mathcal{B}}^{(a)} = 24.08$ for $\theta = 0.1$ and $\overline{\mathcal{B}}^{(b)} = 71.55$ for $\theta = 0.5$. Clearly, the values of Ω and θ affect $\overline{\mathcal{B}}$. Given θ, when Ω is large, data transmit energy α_k in (2) is large. Due to large energy consumption for data transmission, compared to energy harvesting, the battery becomes near empty at its steady-state and SU may stop functioning, due to energy outage. When Ω is small, α_k in (2) is small. Due to small energy consumption for data transmission, compared to energy harvesting, the battery becomes near full at its steady-state, indicating that SU has failed to utilize the excess energy. Both cases inevitably hinder data transmission, leading to a reduction in $R_{\rm LB}$. Similar argument holds true, when θ varies and Ω is given. In particular, when θ is small, transmit energy α_k in (2) is large, and when θ is large, transmit energy α_k in (2) is small. Again, both cases impede data transmission, leading to a lower $R_{\rm LB}$. Overall, the observations we make in Figs. 7, 8, and 9 confirm that optimizing both Ω and θ to achieve a balance between the energy harvesting and the energy consumption for data transmission is of high importance.

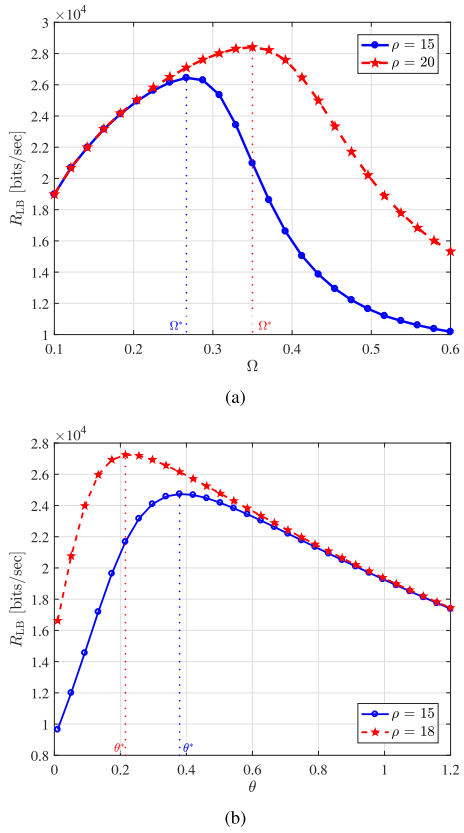

Fig. 7. (a) $R_{\rm LB}$ versus Ω for $K = 80$, $\theta = 0.2$, (b) $R_{\rm LB}$ versus θ for $K = 80$, $\Omega = 0.35$.

Fig. 10(a) illustrates the behavior of $P_b^{\rm Out}$ for a single user in terms of Ω for $\theta = 0.05$. Fig. 10(b) plots $P_b^{\rm Out}$ versus θ for $\Omega = 0.35$. For $\alpha_{\rm t} = 1$, $P_b^{\rm Out}$ in (43) reduces to $P_b^{\rm Out} = \zeta_0 + \zeta_1$, i.e., $P_b^{\rm Out}$ depends on Ω and θ, via only the first two entries of vector $\boldsymbol{\zeta}$. Fig. 10(a) shows that, as Ω increases, $P_b^{\rm Out}$ increases as well. This is because as Ω increases, given θ, α_k in (2) increases. Due to large energy consumption for data transmission the chance of the battery depletion and hence $P_b^{\rm Out}$ increase. Fig. 10(b) demonstrates that, as θ increases, $P_b^{\rm Out}$ decreases. This is because as θ increases, given Ω, α_k in (2) decreases. Due to small energy consumption for data transmission the chance of the battery depletion and hence $P_b^{\rm Out}$ decrease.

Fig. 11(a) shows how $\eta_{\rm EE}$ and $\eta_{\rm SE}$ vary as Ω changes. As Ω increases, both $\eta_{\rm EE}$ and $\eta_{\rm SE}$ increase, until Ω reaches a certain value, denoted as $\Omega^*_{\rm EE}$. We note that at $\Omega = \Omega^*_{\rm EE}$, $\eta_{\rm EE}$ achieves its maximum value. When Ω exceeds $\Omega^*_{\rm EE}$, $\eta_{\rm EE}$

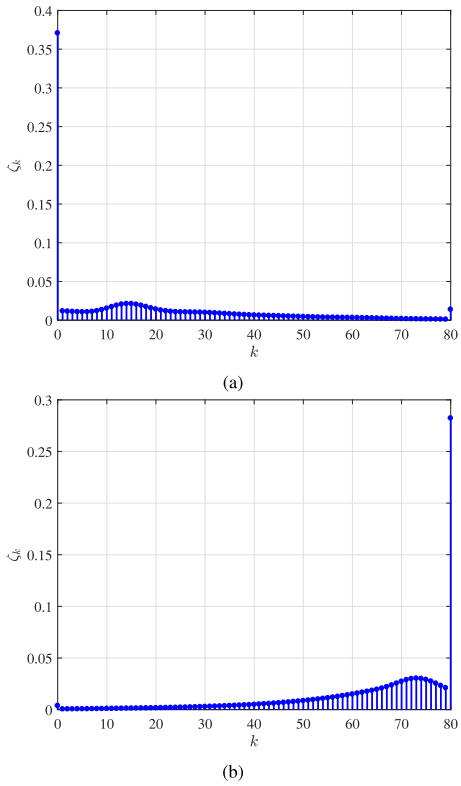

Fig. 8. ζ_k versus k for $K = 80$, $\rho = 15, \theta = 0.2$, (a) $\Omega = 0.45$, (b) $\Omega = 0.30$.

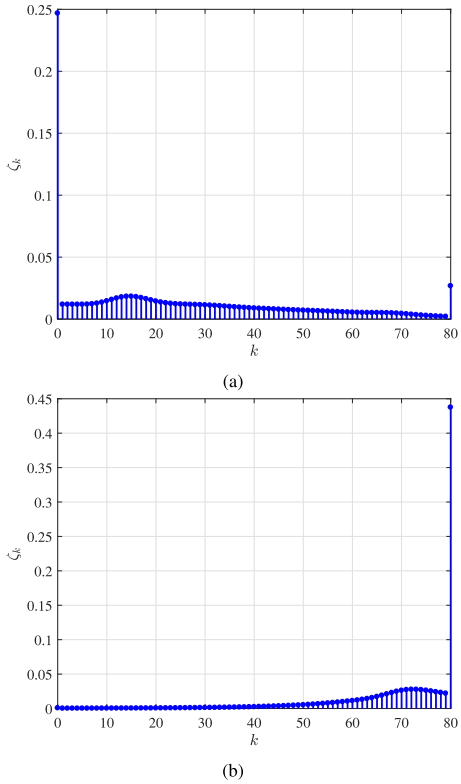

Fig. 9. ζ_k versus k for $K = 80$, $\rho = 15, \Omega = 0.35$, (a) $\theta = 0.1$, (b) $\theta = 0.5$.

decreases while η_{SE} increases. This trend continues until Ω reaches another certain value, denoted as Ω^*_{SE}. We note that at $\Omega = \Omega^*_{\mathrm{SE}}$, η_{SE} achieves its maximum value. When Ω exceeds

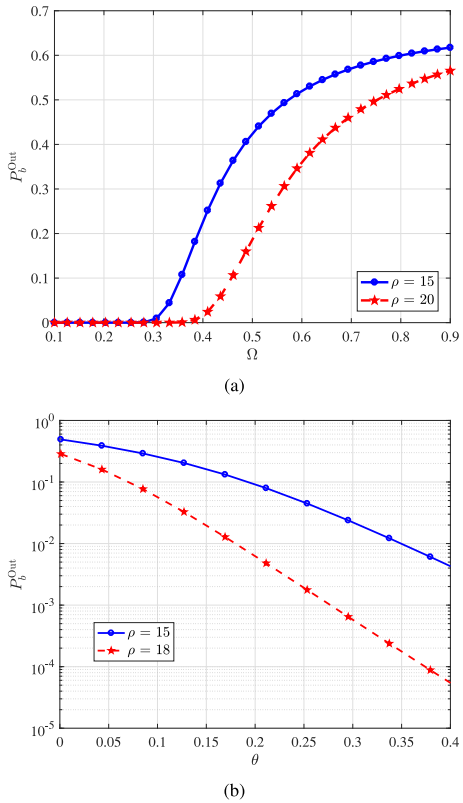

Fig. 10. (a) P_b^{Out} versus Ω for $K = 80$, $\theta = 0.05$, (b) P_b^{Out} versus θ for $K = 80$, $\Omega = 0.35$.

Ω^*_{SE}, both η_{EE} and η_{SE} decrease. We also observe that $\Omega^*_{\mathrm{SE}} > \Omega^*_{\mathrm{EE}}$.

Fig. 11(b) shows how η_{EE} and η_{SE} vary as θ changes. As θ increases, both η_{EE} and η_{SE} increase, until θ reaches a certain value, denoted as θ^*_{SE}. We observe that at $\theta = \theta^*_{\mathrm{SE}}$, η_{SE} achieves its maximum value. When θ exceeds θ^*_{SE}, η_{SE} decreases while η_{EE} increases. This trend continues until θ reaches another certain value, denoted as θ^*_{EE}. When θ exceeds θ^*_{EE}, both η_{EE} and η_{SE} decrease. We also observe that $\theta^*_{\mathrm{SE}} < \theta^*_{\mathrm{EE}}$.

Motivated by [48] we define a new metric, denoted as Z below, which is a weighted summation of η_{SE} and η_{EE}

$$Z = \kappa\eta_{\mathrm{SE}} + (1-\kappa)\eta_{\mathrm{EE}}. \tag{48}$$

where $0 \leq \kappa \leq 1$ is the weighting factor. When $\kappa = 1$, maximizing Z defined in (48) becomes equal to maximizing the spectral efficiency (our problem in (P1)). When $\kappa = 0$, maximizing Z becomes equal to maximizing the energy efficiency. Fig. 12(a) illustrates Z versus Ω for different values of κ. We observe that the value of Ω which maximizes Z is different for different values of κ. Fig. 12(b) illustrates Z versus θ for different values of κ. We observe that the value of θ which maximizes Z is different for different values of κ.

• *Solving Problems ((P1) and $(SP1\text{-}SU_n)$):* Next, we consider solving the constrained optimization problem (P1) and $(\mathrm{SP1\text{-}SU}_n)$ and plot the maximized R_{LB}, denoted as R^*_{LB} (R^*_{LB} is R_{LB} evaluated at the solutions obtained from solving (P1) and $(\mathrm{SP1\text{-}SU}_n)$).

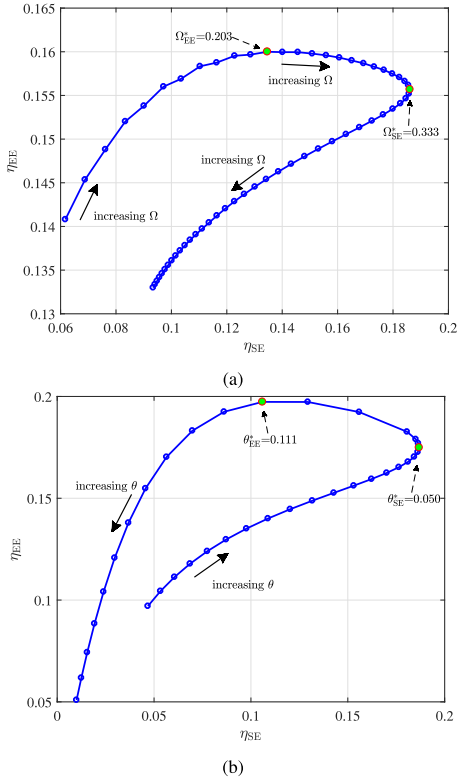

Fig. 11. (a) $\eta_{\rm EE}$ versus $\eta_{\rm SE}$ for different values of Ω and $\theta = 0.02$, (b) $\eta_{\rm EE}$ versus $\eta_{\rm SE}$ for different values of θ and $\Omega = 0.6$.

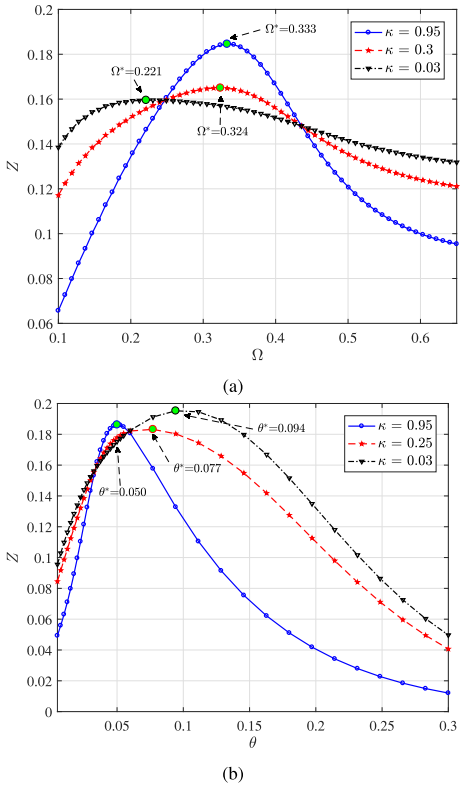

Fig. 12. (a) Z versus Ω for $\theta = 0.02$, (b) Z versus θ for $\Omega = 0.6$.

Fig. 13 depicts $R^*_{\rm LB}$ obtained by solving (P1) and (SP1-SU_n) versus $\overline{I}_{\rm av}$ for $N_{\rm u} = 3, \pi_0 = 0.7, 0.8$. We let the statistics of fading coefficients be different across

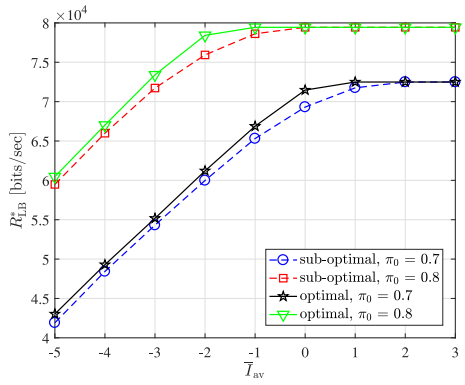

Fig. 13. $R_{\rm LB}$ versus $\overline{I}_{\rm av}$ for $K = 60$, $\rho = 10$, $N_{\rm u} = 3$.

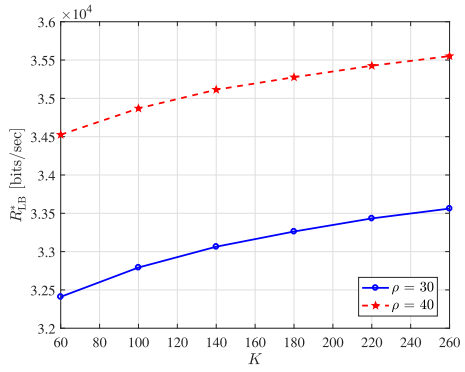

Fig. 14. $R^*_{\rm LB}$ versus K for $\overline{I}_{\rm av} = 2$ dB.

SUs, $\boldsymbol{\gamma} = [2, 2.2, 2.1], \boldsymbol{\delta}_u = [1, 0.8, 1.2], \boldsymbol{\delta}_z = [1, 0.5, 0.8]$ and $K = 60$, $\rho = 10$ be equal for all SUs. We observe that for small $\overline{I}_{\rm av}$ the "sub-optimal" solution obtained from solving (SP1-SU_n) yields a lower sum-rate in comparison to the "optimal" solution obtained from solving (P1). However, for large $\overline{I}_{\rm av}$, when AIC is not active these two solutions become identical. As π_0 increases, the probability of the spectrum being actually idle increases and the opportunity for SUs to utilize the spectrum for data transmission increases. Consequently, the sum-rate lower bound increases as π_0 increases, for a given $\overline{I}_{\rm av}$.

Fig. 14 depicts $R^*_{\rm LB}$ versus K for $N_{\rm u} = 3, \rho = 30, 40$. We observe that as K increases, $R^*_{\rm LB}$ increases. This is expected, since as K increases the chance of energy overflow decreases, leading to a larger amount of stored energy in the battery, which can be utilized to support a higher data rate transmission.

Fig. 15 shows $R^*_{\rm LB}$ versus $\overline{I}_{\rm av}$ for $K = 80$, $\rho = 10, 15$ and $N_{\rm u} = 3$. For small $\overline{I}_{\rm av}$, the AIC in (42) is active and consequently, it limits transmit power of SUs. As $\overline{I}_{\rm av}$ increases, SUs can transmit at higher power levels and $R^*_{\rm LB}$ increases, until $R^*_{\rm LB}$ reaches its maximum value. Increasing $\overline{I}_{\rm av}$ any further, beyond the knee point in Fig. 15, does not increase $R^*_{\rm LB}$. This is because for large $\overline{I}_{\rm av}$, transmit power levels are restricted by the amount of harvested and stored energy in the battery (i.e., they are not restricted by AIC). Therefore, increasing $\overline{I}_{\rm av}$ beyond the knee point has no effect on $R^*_{\rm LB}$. Moreover, for small $\overline{I}_{\rm av}$ where the AIC is active, increasing ρ has no effect

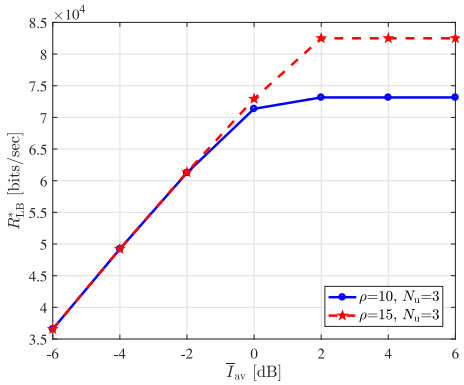

Fig. 15. $R^*_{\rm LB}$ versus $\overline{I}_{\rm av}$ for $N_{\rm u} = 3$, $K = 80$.

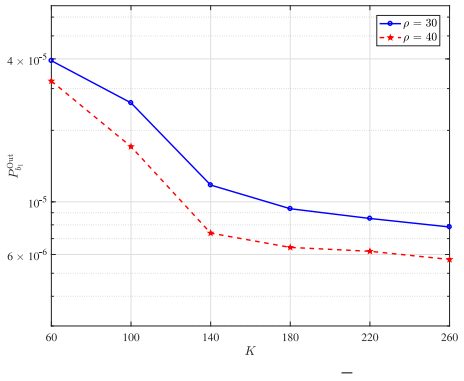

Fig. 16. $P^{\rm Out}_{b_1}$ for $\rm SU_1$ versus K when $\overline{I}_{\rm av} = 2$ dB.

on $R^*_{\rm LB}$. On the other hand, for large $\overline{I}_{\rm av}$, when ρ increases, $R^*_{\rm LB}$ increases.

Considering $\rm SU_1$, Fig 16 depicts $P^{\rm Out}_{b_1}$ of this user versus K where the optimization variables Ω_1 and θ_1 are obtained by solving (P1) and maximizing $R_{\rm LB}$ and then substituting the optimized variables in (43) to calculate $P^{\rm Out}_{b_1}$. We observe that increasing K leads to a lower $P^{\rm Out}_{b_1}$.

We define the transmission outage probability $P^{\rm Out}_{\alpha_n}$ as the probability of $\rm SU_n$ not being able to transmit data to the AP, due to either a weak $\rm SU_n$–AP link with small fading coefficient or insufficient amount of stored energy at the battery. We have

$$P^{\rm Out}_{\alpha_n} = \Pr(P_n = 0|\widehat{\mathcal{H}}_{0,n}) = \omega_{0,n}\Pr(P_n = 0|\widehat{\mathcal{H}}_{0,n}, \mathcal{H}_0) + \omega_{1,n}\Pr(P_n = 0|\widehat{\mathcal{H}}_{0,n}, \mathcal{H}_1), \tag{49}$$

where

$$\Pr\Big(P_n = 0|\widehat{\mathcal{H}}_{0,n}, \mathcal{H}_\varepsilon\Big) = \sum_{k=0}^{\alpha_{\rm t}} \zeta_{k,n}\Pr\Big(\alpha_{k,n} = 0|\widehat{\mathcal{H}}_{0,n}, \mathcal{H}_\varepsilon, \mathcal{B}_n \le \alpha_{\rm t}\Big) + \sum_{k=\alpha_{\rm t}+1}^{K} \zeta_{k,n}\Pr\Big(\alpha_{k,n} = 0|\widehat{\mathcal{H}}_{0,n}, \mathcal{H}_\varepsilon, \mathcal{B}_n \ge \alpha_{\rm t}+1\Big). \tag{50}$$

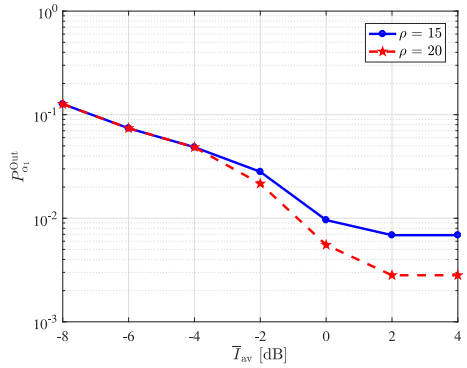

Fig. 17. $P^{\rm Out}_{\alpha_1}$ for $\rm SU_1$ versus $\overline{I}_{\rm av}$ for $\rm SU_1$ when $K = 100$.

Substituting (3) and (50) in (49) we get

$$P^{\rm Out}_{\alpha_n} = \sum_{k=0}^{\alpha_{\rm t}} \zeta_{k,n} + \sum_{k=\alpha_{\rm t}+1}^{K} \zeta_{k,n}\, Y_{k,n}. \tag{51}$$

Fig. 17 shows $P^{\rm Out}_{\alpha_1}$ for $\rm SU_1$ versus $\overline{I}_{\rm av}$ where the optimization variables Ω_1 and θ_1 are obtained by solving (P1) and maximizing $R_{\rm LB}$ and then substituting the optimized variables in (51) to compute $P^{\rm Out}_{\alpha_1}$. Starting from small $\overline{I}_{\rm av}$, as $\overline{I}_{\rm av}$ increases, SUs can transmit at higher power levels and $P^{\rm Out}_{\alpha_1}$ decreases, until $P^{\rm Out}_{\alpha_1}$ reaches its minimum value. Increasing $\overline{I}_{\rm av}$ any further, beyond the knee point in Fig. 17, does not reduce $P^{\rm Out}_{\alpha_1}$. This is because for large $\overline{I}_{\rm av}$ transmit power levels are restricted by the amount of harvested and stored energy in the battery (i.e., they are not restricted by AIC). Therefore, increasing $\overline{I}_{\rm av}$ beyond the knee point has no effect on $P^{\rm Out}_{\alpha_1}$.

VII. Conclusion

We considered an uplink opportunistic CR network, that can access a spectrum band licensed to a primary network. Each SU is equipped with a finite size battery, for storing energy. Modeling the dynamics of the battery as a finite state Markov chain, we established a lower bound on the achievable uplink sum-rate of SUs–AP links, in the presence of both spectrum sensing and channel estimation errors. We proposed a parameterized transmit power control strategy that allows each SU to adapt its power, according to the received feedback information from the AP regarding its link fading coefficient and its stored energy in the battery. We optimized the transmit parameters such that the derived uplink sum-rate lower bound is maximized, subject to AIC. Since the proposed constrained optimization problem is not convex and the objective function and the constraints are not differentiable with respect to the optimization parameters, we resorted to grid-based search methods to solve the problem. We explored the trade-offs between $R_{\rm LB}$, spectrum sensing duration, and channel estimation error. We also illustrated the trade-offs between spectral efficiency and energy efficiency for our CR system. As future work, we plan to study how a non-ideal feedback channel, combined with spectrum sensing and channel estimation errors, will affect our sum-rate maximization problem. In particular, we will consider the effects of $\rm SU_n$'s mobility and bandwidth-limited feedback channel on our optimization problem and its solution.

REFERENCES

[1] T. Yucek and H. Arslan, "A survey of spectrum sensing algorithms for cognitive radio applications," *IEEE Commun. Surveys Tuts.*, vol. 11, no. 1, pp. 116–130, 1st Quart., 2009.

[2] A. Ali and W. Hamouda, "Advances on spectrum sensing for cognitive radio networks: Theory and applications," *IEEE Commun. Surveys Tuts.*, vol. 19, no. 2, pp. 1277–1304, 2nd Quart., 2017.

[3] S. Stotas and A. Nallanathan, "Optimal sensing time and power allocation in multiband cognitive radio networks," *IEEE Trans. Commun.*, vol. 59, no. 1, pp. 226–235, Jan. 2011.

[4] H. Yazdani and A. Vosoughi, "On the spectrum sensing, beam selection and power allocation in cognitive radio networks using reconfigurable antennas," in *Proc. 53rd Annu. Conf. Inf. Sci. Syst. (CISS)*, Baltimore, MD, USA, Mar. 2019, pp. 1–7.

[5] H. Yazdani, A. Vosoughi, and X. Gong, "Beam selection and discrete power allocation in opportunistic cognitive radio systems with limited feedback using ESPAR antennas," *IEEE Trans. Cogn. Commun. Netw.*, vol. 6, no. 1, pp. 325–339, Mar. 2020.

[6] H. Yazdani, A. Vosoughi, and X. Gong, "Achievable rates of opportunistic cognitive radio systems using reconfigurable antennas with imperfect sensing and channel estimation," 2020. [Online]. Available: arXiv:2007.04390.

[7] S. Mao, M. H. Cheung, and V. W. S. Wong, "Joint energy allocation for sensing and transmission in rechargeable wireless sensor networks," *IEEE Trans. Veh. Technol.*, vol. 63, no. 6, pp. 2862–2875, Jul. 2014.

[8] S. Yin, Z. Qu, and S. Li, "Achievable throughput optimization in energy harvesting cognitive radio systems," *IEEE J. Sel. Areas Commun.*, vol. 33, no. 3, pp. 407–422, Mar. 2015.

[9] S. Biswas, S. Dey, and A. Shirazinia, "Sum throughput maximization in a cognitive multiple access channel with cooperative spectrum sensing and energy harvesting," *IEEE Trans. Cogn. Commun. Netw.*, vol. 5, no. 2, pp. 382–399, Jun. 2019.

[10] M.-L. Ku, W. Li, Y. Chen, and K. J. R. Liu, "Advances in energy harvesting communications: Past, present, and future challenges," *IEEE Commun. Surveys Tuts.*, vol. 18, no. 2, pp. 1384–1412, 2nd Quart., 2016.

[11] H. Zhang, Y. Nie, J. Cheng, V. C. M. Leung, and A. Nallanathan, "Sensing time optimization and power control for energy efficient cognitive small cell with imperfect hybrid spectrum sensing," *IEEE Trans. Wireless Commun.*, vol. 16, no. 2, pp. 730–743, Feb. 2017.

[12] L. Zhang, M. Xiao, G. Wu, S. Li, and Y.-C. Liang, "Energy-efficient cognitive transmission with imperfect spectrum sensing," *IEEE J. Sel. Areas Commun.*, vol. 34, no. 5, pp. 1320–1335, May 2016.

[13] K. Wu, H. Jiang, and C. Tellambura, "Sensing, probing, and transmitting strategy for energy harvesting cognitive radio," in *Proc. IEEE Int. Conf. Commun. (ICC)*, Paris, France, May 2017, pp. 1–6.

[14] W. Chung, S. Park, S. Lim, and D. Hong, "Optimal transmit power control for energy-harvesting cognitive radio system," in *Proc. IEEE 78th Veh. Technol. Conf. (VTC Fall)*, Las Vegas, NV, USA, Sep. 2013, pp. 1–5.

[15] A. Sultan, "Sensing and transmit energy optimization for an energy harvesting cognitive radio," *IEEE Wireless Commun. Lett.*, vol. 1, no. 5, pp. 500–503, Oct. 2012.

[16] F. Zhang, T. Jing, Y. Huo, and K. Jiang, "Throughput maximization for energy harvesting cognitive radio networks with finite horizon," in *Proc. 9th Int. Conf. Wireless Commun. Signal Process. (WCSP)*, Nanjing, China, Oct. 2017, pp. 1–7.

[17] G. Ardeshiri, H. Yazdani, and A. Vosoughi, "Optimal local thresholds for distributed detection in energy harvesting wireless sensor networks," in *Proc. IEEE Global Conf. Signal Inf. Process. (GlobalSIP)*, Anaheim, CA, USA, Nov. 2018, pp. 813–817.

[18] G. Ardeshiri, H. Yazdani, and A. Vosoughi, "Power adaptation for distributed detection in energy harvesting WSNs with finite-capacity battery," in *Proc. IEEE Global Commun. Conf. (GLOBECOM)*, Waikoloa, HI, USA, 2019, pp. 1–6.

[19] S. Park, H. Kim, and D. Hong, "Cognitive radio networks with energy harvesting," *IEEE Trans. Wireless Commun.*, vol. 12, no. 3, pp. 1386–1397, Mar. 2013.

[20] S. Park and D. Hong, "Achievable throughput of energy harvesting cognitive radio networks," *IEEE Trans. Wireless Commun.*, vol. 13, no. 2, pp. 1010–1022, Feb. 2014.

[21] D. Zhang *et al.*, "Energy-harvesting-aided spectrum sensing and data transmission in heterogeneous cognitive radio sensor network," *IEEE Trans. Veh. Technol.*, vol. 66, no. 1, pp. 831–843, Jan. 2017.

[22] H. S. Lee, M. E. Ahmed, and D. I. Kim, "Optimal spectrum sensing policy in RF-powered cognitive radio networks," *IEEE Trans. Veh. Technol.*, vol. 67, no. 10, pp. 9557–9570, Oct. 2018.

[23] D. Niyato, P. Wang, and D. I. Kim, "Performance analysis of cognitive radio networks with opportunistic RF energy harvesting," in *Proc. IEEE Global Commun. Conf.*, Austin, TX, USA, 2014, pp. 1096–1101.

[24] D. Altinel and G. K. Kurt, "Finite-state Markov channel based modeling of RF energy harvesting systems," *IEEE Trans. Veh. Technol.*, vol. 67, no. 2, pp. 1713–1725, Feb. 2018.

[25] X. Yang, M. Sheng, H. Sun, X. Wang, and J. Li, "Spatial throughput analysis and transmission strategy design in energy harvesting cognitive radio networks," *IEEE Trans. Commun.*, vol. 66, no. 12, pp. 5938–5951, Dec. 2018.

[26] S. Park, J. Heo, B. Kim, W. Chung, H. Wang, and D. Hong, "Optimal mode selection for cognitive radio sensor networks with RF energy harvesting," in *Proc. IEEE 23rd Int. Symp. Pers. Indoor Mobile Radio Commun. (PIMRC)*, Sydney, NSW, Australia, 2012, pp. 2155–2159.

[27] J. Yan and Y. Liu, "A dynamic SWIPT approach for cooperative cognitive radio networks," *IEEE Trans. Veh. Technol.*, vol. 66, no. 12, pp. 11122–11136, Dec. 2017.

[28] F. Zhou, Z. Li, J. Cheng, Q. Li, and J. Si, "Robust AN-aided beamforming and power splitting design for secure MISO cognitive radio with SWIPT," *IEEE Trans. Wireless Commun.*, vol. 16, no. 4, pp. 2450–2464, Apr. 2017.

[29] M. R. Zenaidi, Z. Rezki, and M.-S. Alouini, "On communications under stochastic energy harvesting with noisy channel state information," in *Proc. IEEE Global Commun. Conf. (GLOBECOM)*, Washington, DC, USA, 2016, pp. 1–6.

[30] R. Ma and W. Zhang, "Optimal power allocation for energy harvesting communications with limited channel feedback," in *Proc. IEEE Global Conf. Signal Inf. Process. (GlobalSIP)*, Atlanta, GA, USA, 2014, pp. 193–197.

[31] A. H. Sakr and E. Hossain, "Cognitive and energy harvesting-based D2D communication in cellular networks: Stochastic geometry modeling and analysis," *IEEE Trans. Commun.*, vol. 63, no. 5, pp. 1867–1880, May 2015.

[32] M.-L. Ku, Y. Chen, and K. J. R. Liu, "Data-driven stochastic models and policies for energy harvesting sensor communications," *IEEE J. Sel. Areas Commun.*, vol. 33, no. 8, pp. 1505–1520, Aug. 2015.

[33] M. R. Zenaidi, Z. Rezki, and M.-S. Alouini, "Performance limits of online energy harvesting communications with noisy channel state information at the transmitter," *IEEE Access*, vol. 5, pp. 1239–1249, 2017.

[34] B. Hassibi and B. M. Hochwald, "How much training is needed in multiple-antenna wireless links?" *IEEE Trans. Inf. Theory*, vol. 49, no. 4, pp. 951–963, Apr. 2003.

[35] M. Medard, "The effect upon channel capacity in wireless communications of perfect and imperfect knowledge of the channel," *IEEE Trans. Inf. Theory*, vol. 46, no. 3, pp. 933–946, May 2000.

[36] M. Shirazi and A. Vosoughi, "On distributed estimation in hierarchical power constrained wireless sensor networks," *IEEE Trans. Signal Inf. Process. Netw.*, vol. 6, pp. 442–459, May 2020, doi: 10.1109/TSIPN.2020.2995046.

[37] H. R. Ahmadi and A. Vosoughi, "Impact of wireless channel uncertainty upon distributed detection systems," *IEEE Trans. Wireless Commun.*, vol. 12, no. 6, pp. 2566–2577, Jun. 2013.

[38] A. Vosoughi and Y. Jia, "How does channel estimation error affect average sum-rate in two-way amplify-and-forward relay networks?" *IEEE Trans. Wireless Commun.*, vol. 11, no. 5, pp. 1676–1687, May 2012.

[39] Y. Jia and A. Vosoughi, "Transmission resource allocation for training based amplify-and-forward relay systems," *IEEE Trans. Wireless Commun.*, vol. 10, no. 2, pp. 450–455, Feb. 2011.

[40] Y. Dong, J. Wang, B. Shim, and D. I. Kim, "DEARER: A distance-and-energy-aware routing with energy reservation for energy harvesting wireless sensor networks," *IEEE J. Sel. Areas Commun.*, vol. 34, no. 12, pp. 3798–3813, Dec. 2016.

[41] J. F. Shortle, J. M. Thompson, D. Gross, and C. M. Harris, *Fundamentals of Queueing Theory*, vol. 399. Hoboken, NJ, USA: Wiley, 2018.

[42] R. Zhang, H. Chen, P. L. Yeoh, Y. Li, and B. Vucetic, "Full-duplex cooperative cognitive radio networks with wireless energy harvesting," in *Proc. IEEE Int. Conf. Commun. (ICC)*, Paris, France, 2017, pp. 1–6.

[43] X. Guo, Y. He, S. Atapattu, S. Dey, and J. S. Evans, "Power allocation for distributed detection systems in wireless sensor networks with limited fusion center feedback," *IEEE Trans. Commun.*, vol. 66, no. 10, pp. 4753–4766, Oct. 2018.

[44] H. Yazdani and A. Vosoughi, "On optimal sensing and capacity tradeoff in cognitive radio systems with directional antennas," in *Proc. IEEE Global Conf. Signal Inf. Process. (GlobalSIP)*, Anaheim, CA, USA, Nov. 2018, pp. 1015–1019.

[45] S. M. Kay, *Fundamentals of Statistical Signal Processing*. Upper Saddle River, NJ, USA: Prentice-Hall PTR, 1993.
[46] A. Goldsmith, *Wireless Communications*. Cambridge, U.K.: Cambridge Univ. Press, 2005.
[47] A. Vosoughi and A. Scaglione, "On the effect of receiver estimation error upon channel mutual information," *IEEE Trans. Signal Process.*, vol. 54, no. 2, pp. 459–472, Feb. 2006.
[48] T.-Q. Wu, H.-C. Yang, and Y.-C. Liang, "Cooperative secondary beam selection for cognitive multiuser MIMO transmission with random beamforming," *IEEE Trans. Cogn. Commun. Netw.*, vol. 2, no. 2, pp. 141–149, Jun. 2016.

Hassan Yazdani received the B.Sc. degree (Hons.) in electrical engineering from the Shiraz University of Technology, Shiraz, Iran, in 2009, and the M.Sc. degree in electrical engineering from the University of Tehran, Tehran, Iran, in 2012. He is currently pursuing the Ph.D. degree in electrical engineering with the University of Central Florida. His current research interests include cognitive radio, statistical signal processing, energy harvesting in wireless sensor networks, and array signal processing.

Azadeh Vosoughi (Senior Member, IEEE) received the B.S. degree in electrical engineering from the Sharif University of Technology, Tehran, Iran, in 1997, the M.S. degree in electrical engineering from Worcester Polytechnic Institute, Worcester, MA, USA, in 2001, and the Ph.D. degree in electrical engineering from Cornell University, Ithaca, NY, USA, in 2006. She is an Associate Professor with the Department of Electrical and Computer Engineering, University of Central Florida. Her research interests lie in the general areas of wireless communications, statistical signal processing, distributed detection and estimation theory, and brain signal processing. She received the NSF CAREER Award in 2011.